BIG – Branschsamverkan i grunden

Forskningsprogram för effektiv och säker grundläggning av vägar och järnvägar

Projekt A2017:14

Changes in undrained shear strength as a function of time under embankments

Final report

KTH ROYAL INSTITUTE OF TECHNOLOGY

CHALMERS UNIVERSITY OF TECHNOLOGY

TRAFIKVERKET

STATENS GEOTEKNISKA INSTITUT

LULEÅ TEKNISKA UNIVERSITET

BIG – Branschsamverkan i grunden
Forskningsprogram för effektiv och säker grundläggning av vägar och järnvägar

Rapport BIG projekt A2017:14

Changes in undrained shear strength as a function of time under embankments

Final report

Hannes Hernvall

CHALMERS

Framtagen inom ramen för BIG av Chalmers tekniska högskola

Göteborg 2021

Rapport publicerad av BIG, Branschsamverkan i grunden
Beställning Web: www.big-geo.se

ISBN 978-91-986926-5-5
Upplaga Digital

Framtagen av Chalmers tekniska högskola
Department of Architecture and Civil Engineering
Geology & Geotechnics
Författare Hannes Hernvall

CHALMERS

A2017-14: Changes in undrained shear strength as a function of time under embankments

HANNES HERNVALL

Department of Architecture and Civil Engineering
Geology & Geotechnics
CHALMERS UNIVERSITY OF TECHNOLOGY
Göteborg, Sweden 2021

TECHNICAL REPORT GEOTECHNICAL ENGINEERING

A2017-14: Changes in undrained shear strength as a function of time under embankments

HANNES HERNVALL

Department of Architecture and Civil Engineering
Geology & Geotechnics
CHALMERS UNIVERSITY OF TECHNOLOGY
Göteborg, Sweden 2021

A2017-14: Changes in undrained shear strength as a function of time under embankments
HANNES HERNVALL
ISBN n/a

Technical report A2017-14
ISSN n/a
Department of Architecture and Civil Engineering
Geology & Geotechnics
Chalmers University of Technology
SE-412 96 Göteborg
Sweden

Göteborg, Sweden 2021

A2017-14: Changes in undrained shear strength as a function of time under embankments
Technical report Geotechnical Engineering
HANNES HERNVALL
Department of Architecture and Civil Engineering
Geology & Geotechnics
Chalmers University of Technology

Abstract

A methodology to evaluate the changes of undrained shear strength in the sub-soil as a function of time under the centreline of an embankment was developed. This is based on model simulations, using the instrumented test embankment in Haarajoki, Finland, as a case study. The simulations demonstrate that the evolution of the undrained strength under embankment loading as a function of time is complicated. Firstly, the evolution of strength is related to both consolidation and creep, which are strongly affected by the apparent preconsolidation pressure and the creep parameters. Any significant gains in strength are only possible when the effective stresses go beyond the normal consolidation surface. Furthermore, the degradation of bonding in sensitive clays may in the short term reduce the undrained shear strength, in particular if the preconsolidation pressure is only marginally exceeded. Most importantly, the results also identify gaps in our knowledge, with regards of the role of the evolution and anisotropy and principal stress rotation on the evolving undrained shear strength, which affect the strength mobilisation in most of the failure surface.

Keywords: embankment, natural clay, undrained shear strength, numerical modelling

Contents

1 Introduction

Linear infrastructure on embankments is a fundamental part of our transport infrastructure today. Many of the existing road and railway embankments are located on soft, and often sensitive, clays and have been in service for several decades. The old embankments are in many cases built directly on the natural soil, without any ground improvement. The current stability of these embankments is to a large extent unknown, as is how the stability has changed over time. With changing intensity of traffic and increasing axle loads as well as climate change induced environmental loads, it is necessary to be able to asses the change in stability of embankments on soft soils.

In the last 60 years numerous research has been published on embankments on soft soils for both the serviceability limit state (Berre 2014; Ladd et al. 1994; Karstunen et al. 2005; Larsson and Mattsson 2003) and the ultimate limit state (Berre 2018; Lehtonen et al. 2015; Rochelle et al. 1974; Zwanenburg et al. 2012). An important part in assessing the stability of embankments is to quantify the mobilised undrained shear strength s_u of the soil. The mobilised s_u is one of the emerging soil properties used in stability analyses of embankments on soft soils. The change in undrained shear strength s_u over time under embankments, considering different loading directions, has however not been investigated in greater detail. Some of the research investigating the changes in undrained shear strength with time includes Vepsäläinen et al. (2002), D'Ignazio (2016), Larsson and Mattsson (2003), and Lundström and Dehlbom (2019). The results on Murro test embankment suggest that there are cases where the undrained shear strength might even reduce in time (Koskinen and Karstunen 2006). This reduction of undrained shear strength is associated with destructuration in sensitive soft clays.

With the exception of Lundström and Dehlbom (2019), as far as the Authors are aware, there have not been much quantitative attempts to develop methodologies to evaluate the change in undrained shear strength over time. Lundström and Dehlbom (2019) propose a methodology that relies on settlement analyses in combination with assumptions made on the apparent preconsolidation pressure and the coefficient of lateral earth pressure at rest, and various empirical relations between the undrained shear strength in different directions. The methodology was tested on two different railway sections. However, when the undrained shear strengths measured in the laboratory under axisymmetric conditions are applied to plane strain condition uncertainties follow. As an embankment of soft clay is most often not a one dimensional problem, in particular narrow old railways embankments, even "correct" predictions of vertical settlements do not imply that the system has been modelled correctly. Furthermore, the mobilised undrained shear strength is also affected by the rotation of the principal stress axes under the side slopes of the embankment, which is the area where the failure surface often initiates. This is not something that can be captured by empirical relations, or indeed by axisymmetric testing in laboratory. However, the time-dependent mobilisation of strength in different directions comes out automatically in effective stress based numerical analyses, as done in this report, provided the model used can be shown to be able to model the behaviour of the system. The focus of Lundström and Dehlbom (2019) has been on (very) old embankments (¿ 150 year), where the primary consolidation has been completed, whilst the embankment studied in this report is rather young, with significant excess pore pressured remaining.

The aim of this project is to use the results from state-of-the-art soil modelling in a monitored test embankment to understand how the evolution of anisotropy, and the possible

degradation of the mobilised undrained shear strength, in sensitive clays may affect the stability of embankments. This report presents a methodology to evaluate the changes of undrained shear strength in the sub-soil as a function of time, based on model simulations, using the instrumented test embankment in Haarajoki, Finland, as a case study.

2 Haarajoki test embankment

Haarajoki test embankment was built in 1997 by the Finnish Transport Administration to improve the understanding on the development of long term settlements, horizontal deformations and the dissipation of excess pore pressures. Haarajoki test embankment is located in Southern Finland, about 40 km north-east of Helsinki. In conjunction, an international competition was held, were practitioner were invited to predict the deformations of the test embankment two years after the construction (Lojander and Vepsäläinen 2001). This highlighted how poor the settlement predictions in general are.

About three years after the construction of Haarajoki embankment, a subsequent mainly experimental study aimed to quantify how the undrained shear strength had changed in time, due to the significant consolidation under the embankment (Vepsäläinen et al. 2002). The results of the study were inconclusive, with only a slight increase measured/estimated in one part and not at all in the other parts. Samples taken from beneath the embankment showed a decrease in water content (w) in the first five meters, but very small changes, if any, in the deeper parts of the deposit. After these initial studies, the embankment has been used to evaluate and benchmark constitutive soil models (Yildiz et al. 2009; Amavasai et al. 2017), since it is a well documented case, with both laboratory and field monitoring data available.

2.1 Site conditions

Haarajoki test embankment is situated on a deposit of soft and sensitive clay with a thickness of around 20 meters. A two meter thick dry crust is located just under the ground surface, followed by soft clay, and beneath the clay deposit there is some frictional material in form of a glacial till. Based on the measurements in the site, the groundwater table is located at the ground surface, and an excess pore pressure between 3 to 10 kPa has been measured in the area (Näätänen and Lojander 1998). The sensitivity of the clays ranges from 25 in the top of the deposit to 50 in the bottom. The undrained shear strength s_u, based on fall cone and field vane tests, is around 20 kPa for the first 8 meters, and subsequently increases with about 0.5 kPa/m. The clay has an in situ water content (w) in excess of 100% (significantly over the liquid limit (w_L)) just under the dry crust, with a decrease to 75% at 15 meters depth. With the exception of the dry crust, the water content is either around the liquid limit W_L or just above it, as would be expected for a sensitive clay. The top part of the soft clay deposit, as well as the dry crust are slightly overconsolidated with an overconsolidation ratio (OCR) between 1.5 to 2 and over. The deeper parts of the deposit, from five meters and down, appear to be less overconsolidated, but still there is a pre-overburden pressure of around 20 to 30 kPa, consistent with past changes in the groundwater level. An overview of the soil profile is shown in Figure 2.1.

2.2 Test embankment

Haarajoki embankment was built as a continuous embankment in two parts, one part (50 m) on natural soil and the other part (50 m) on clay improved with pre-fabricated vertical drains (PVDs). In total the embankment is 100 meters long, 2.9 meters high, 8 meters wide on top and 18 meters wide at the bottom, with stabilising berms on each side. The slopes have an

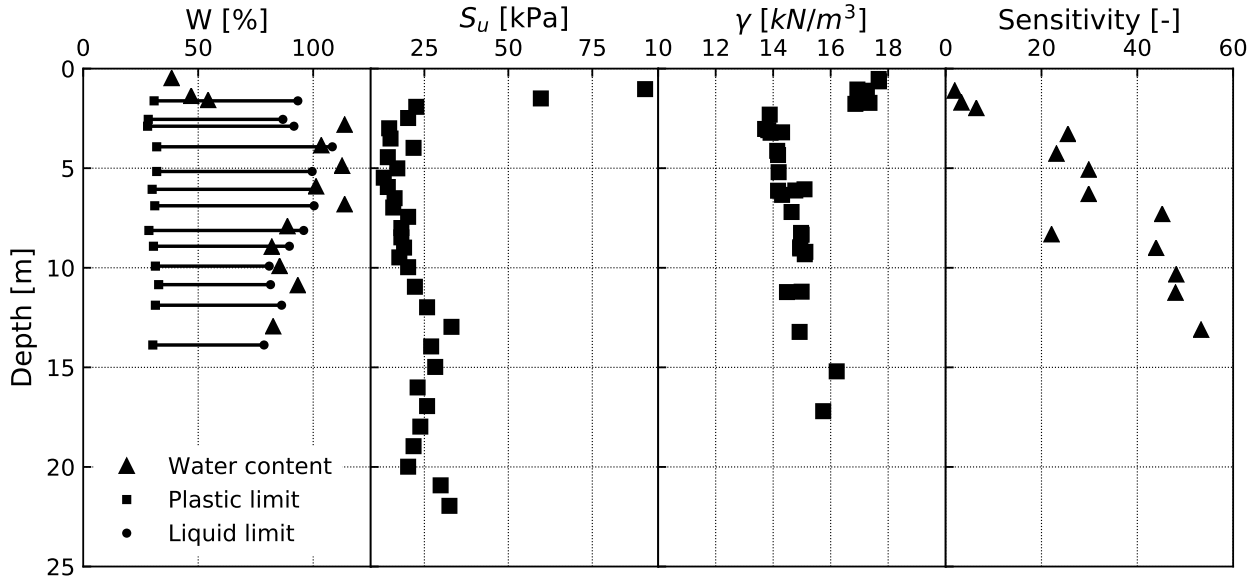

Figure 2.1: *Index properties of the soil beneath Haarajoki test embankment. The undrained shear strength s_u and sensitivity S_t above are derived from fall cone tests.*

approximate inclination of 1:2. The embankment was built in six stages, each of 0.5 meters over a period of 35 days. A working platform of 0.5 meters of fill was placed first, then left to consolidate for 20 days. After that the embankment was raised and compacted with 0.5 meter layers over two days periods until the design height was reached. Two sections, one for each part of the embankment (natural soil vs. PVDs), were instrumented with settlement plates, inclinometers and piezometers.

In hindsight, when looking at the measured longitudinal settlements in (Lojander and Vepsäläinen 2001), the part of the embankment with PVDs has affected the part without drains. Obviously, the instrumentation plan did not consider the 3D effects. This means that the measured settlements (as a function of time) in the part without PVDs are probably slightly larger than they would have been if the entire embankment was built without any vertical drains. Four years after construction, the section without PVDs had settled around 400 mm, while the section with PVDs had settled a bit over 700 mm.

2.3 Soil tests

As part of the site characterisation in situ and laboratory testing was performed. The in situ tests included field vane test (FVT), cone penetration test with pore pressure measurement (CPTu), standard penetration tests (SPT) and Swedish weight sounding. The index tests included density/unit weight, void ratio (e_0), plastic and liquid limit, water content, undrained shear strength with fall cone, sensitivity S_t and organic content. Some of the these properties against depth are shown in Figure 2.1.

Several types of laboratory tests were done to enable to analyse the performance of the embankment, both with conventional techniques and numerical analyses. The types and number of tests performed are shown in Table 2.1. The s_u values from the anisotropically consolidated undrained CAUC tests (performed using strain rates of 0.01-0.1 %/h) were concentrated on the

top 7 m and yield values that are comparable with s_u values measured with field vane and fall cone tests. The results from CAUC and CAUD tests were used to estimate the values for the stress ratio at critical state M_c. There were no direct shear tests available, and from modelling point of view, unfortunately no triaxial tests in extension were made. From the incrementally loaded (IL) oedometer tests, model parameters such as the modified intrinsic compression index λ_i^*, modified swelling index κ^* and the preconsolidation pressure $\sigma' c$ were evaluated. The CRS tests were mainly used to evaluate the coefficient of hydraulic conductivity k, both in the vertical and horizontal direction, as the correction of the strain-rate effects is difficult without data at different strain rates. To determine the horizontal hydraulic conductivity, the samples were rotated 90° before mounting and testing in the CRS oedometers.

Table 2.1: The laboratory test performed. CAUC: Consolidated Anisotropically Undrained Compression, CADC: Consolidated Anisotropically Drained Compression, CRS: Constant Rate of Strain

Test	Number	Parameters
IL	30	λ_i^*, κ^*, σ_c'
CRS	23	k_v, k_h
CAUC	7	M_c, ν'
CADC	10	M_c, ν'

3 Methodology

The undrained shear strength s_u is an emerging property that is dependent on several factors, such as initial effective stresses and the stress path, but also on strain rate and temperature etc. Since the mobilised undrained shear strength of sensitive clays is different in compression and extension (i.e. either anisotropic or dependant on the loading direction), thinking of how the undrained shear strength is determined is very important. Especially under embankments, there are significant stress rotations under the slopes. Therefore, the mobilised undrained shear strength s_u is not a constant soil property and varies along the failure surface. Furthermore, the peak values of s_u are arrived at different shear strains. Often, if total stress based models are used in stability analyses, anisotropy is accounted for by using results from different laboratory tests (triaxial compression, extension, direct shear) for different parts of the sub-soil, ignoring any strain compatibility. Figure 3.1 gives the classic example of which tests that are most relevant for different parts of the failure surface (Bjerrum 1972). Fundamentally, the figure is erroneous, as axisymmetric conditions do not apply in the case of a long embankment. In contrast, in the effective stress-based models, the mobilised strength at a given location at a given time is predicted by the hydro-mechanical coupling of the selected constitutive model, linking the evolution of effective stresses resulting from consolidation with compression and creep. and thus the mobilised undrained shear strength s_u results automatically from the model used. The accuracy depends of course on how well the constitutive model is able to model the soil behaviour and the pore pressure development in the field. If the prediction of pore pressures is off, the predicted mobilised undrained shear strength will also be off.

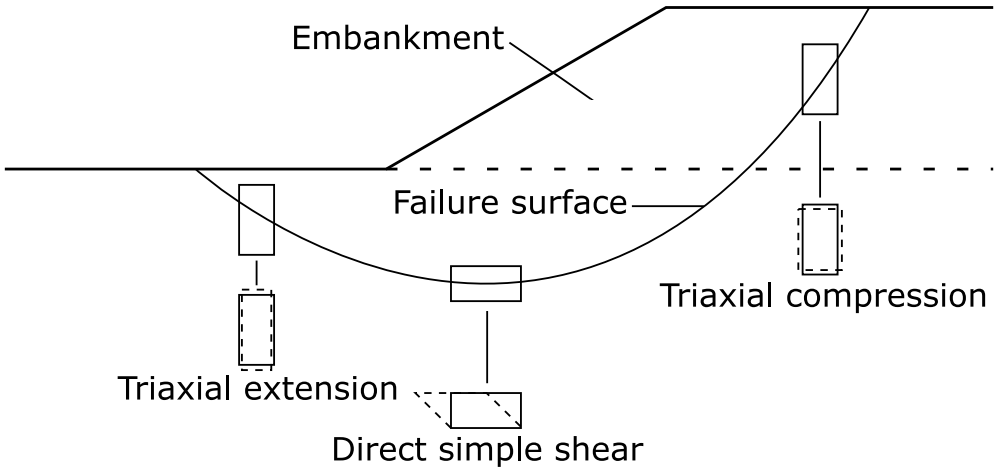

Figure 3.1: *Relevant laboratory soil tests for different parts of the failure surface based on figure by Bjerrum (1972).*

The methodology used to investigate the time-dependent development of the undrained shear strength s_u under an embankment has four steps which are presented in Figure 3.2. It should be noted that whilst the methodology is general, in this report, it has only been applicable for stress points under the centreline of the embankment, where there is no rotation of principal stress axes. The state of stresses (and fabric in an anisotropic soil) for the points in areas with principal stress rotations would namely need to be modelled as a full 3D boundary value problem, as the numerical "sample" no longer has cross-anisotropy, and would deform

differently in different directions as well along the "sample" height.

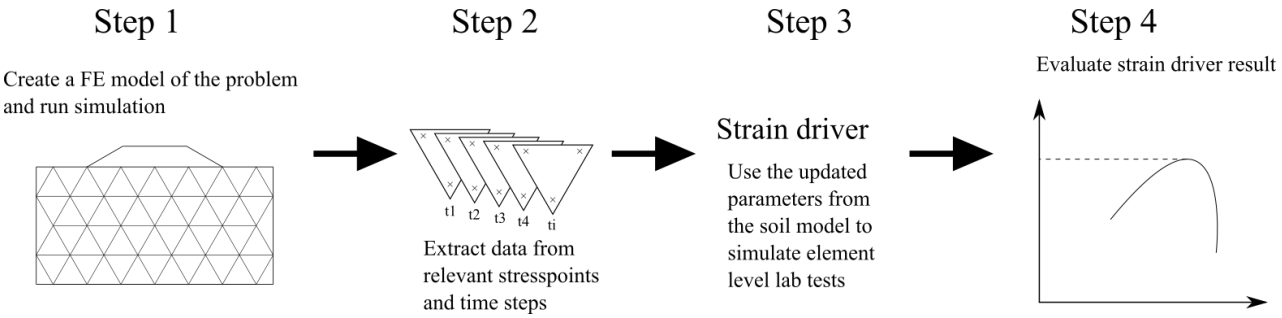

Figure 3.2: *Schematic of the methodology to evaluate the undrained shear strength at different times steps.*

In the first step, a model of the geotechnical problem is created in a Finite Element code (FE). To do this, it is necessary to have a representative constitutive model, with the capabilities to model the essential features of the behaviour of soft sensitive clays. An important part is to extract the relevant model parameters from the necessary soil laboratory tests, and then validate the applicability of the parameters through element level simulations of these laboratory tests with the constitutive model. The same set of parameter need to be used for simulating different tests on the same material (soil layer). When there is confidence in the values of the model parameters, you can run the FE model of the problem at field scale, refining the mesh until the results converge. This FE model should be validated against field measurements to have confidence that the model is able to capture the behaviour of the system to be modelled. In the case of an embankment, the measurements ideally include a combination of vertical settlements (both at the surface and the underground), horizontal movements and excess pore pressures, ideally with piezometers at several different levels to ensure that the whole system is realistically represented. If the results of the FE model differ too much from the field measurements, the potential sources for them need to be investigated. Based on these further adjustments are necessary to calibrate the FE model. When the model is deemed to be accurate enough, it is finally time for step two. Step 1 is the most important, and the most time-consuming, stage in the process. Often the parameters for the dry crust in particular need adjustment to produce representative results.

In step two, the data needed for further modelling is extracted. What data to extract depends on the constitutive model used to model the soil behaviour. For Haarajoki test embankment Creep-SCLAY1S (Sivasithamparam et al. 2015; Gras et al. 2018) was used to simulate the behaviour of the soft clay deposit, given the performance of the model has already been demonstrated for embankment problems (Sivasithamparam et al. 2015; Amavasai et al. 2017; Amavasai et al. 2018).

Under the centreline there are no stress rotations. Thus data that were extracted include the vertical and horizontal effective stresses (note that the two horizontal components are not be equal in a plane strain problem), size of the Normal Compression Surface (linked to the overconsolidation ratio at a given time), as well as the state parameters describing the anisotropy and structure. When dealing with time-dependent response, associated with consolidation and creep, several different time steps can be of interest to see how the undrained shear strength is predicted to develop with time. In such cases, it is necessary to extract the relevant data and parameters from the same data point for several time steps. Under

the centreline, the conditions are thus quite close to a 1D case. For other points, both the effective stress tensor and the fabric tensor need to be extracted in addition to the other state variables and any triaxial/other laboratory test needs to be modelled as a full 3D boundary value problem. As already discussed, this was not done for the case investigated. In the third step the lab tests are simulated at element level with the parameters for initial state from step 2. The test simulated here depends on, of course, on what you are after. In this case undrained triaxial tests in compression and extension together with (undrained) direct simple shear tests were simulated to complement the Swedish practice. This way we can simulate the changes in the anisotropic undrained shear strength of the soft sensitive clay, similarly to Figure 3.1.

Finally, in step number four the simulations of the tests are critically evaluated. It is important not just to look at the computed undrained shear strengths at a given time, but to normalise these with the initial s_u values predicted with the model. If there are any field or laboratory tests associated with measuring changes in the undrained shear strength, these should be compared with the simulated results.

4 Numerical model

The numerical model used for the calculations was created in the FE code Plaxis 2D. Two different constitutive models were used to model the behaviour of the soils, Creep-SCLAY1S (Gras et al. 2018; Sivasithamparam et al. 2015) and a Mohr-Coulomb based model. Creep-SCLAY1S was used to model the deposit of soft and sensitive clay, and was used for five layers in the model. A Mohr-Coulomb model was used to model the embankment, dry crust and the glacial till underneath the clay deposit. The reason for using a Mohr-Coulomb model was too decrease the complexity of the overall model, especially since the properties of the dry crust and the glacial till are rather uncertain.

The numerical model has the following dimensions -100 to +100 in the horizontal direction and from +3 to -25 in the vertical direction. The FE model consisted of 3649 15-noded elements. Following the best practice, the mesh was refined under the embankment to get more accurate results in the area of interest. A cross section of the mesh can be seen in Figure 4.1. Note that in the Serviceability Limit State (SLS) simulations symmetry could be assumed, but for the Ultimate Limit State (ULS) analyses this no longer holds. Furthermore, in the SLS simulations, the traffic load is zero. For ULS analyses, symmetry no longer applies, and traffic load needs to be incorporated. Furthermore, to direct the failure mode to one side of the embankment in otherwise rather symmetric conditions, an imaginary ditch has been added on the right side of the embankment.

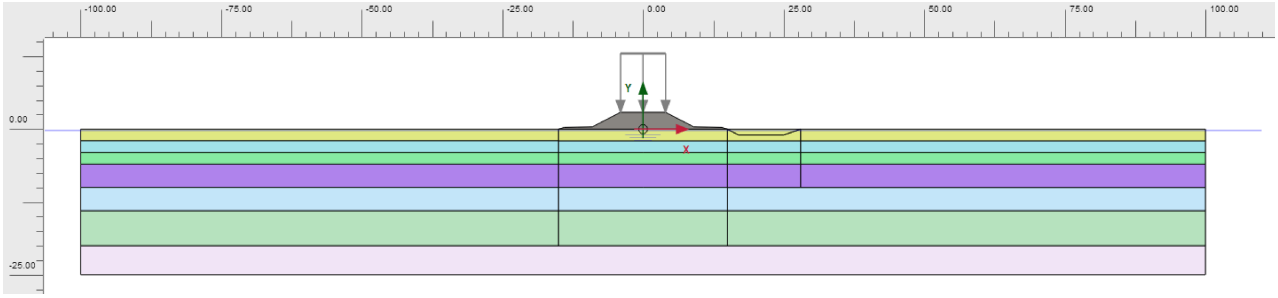

Figure 4.1: *Cross section of the numerical model for Haarajoki embankment in Plaxis 2D.*

4.1 Model parameters for Creep-SCLAY1S

Creep-SCLAY1S requires values for 10 model parameters as listed in Table 4.2. In addition, the reference time τ needs to be chosen to match the loading-rate in the oedometer tests from which POP (or OCR) is determined. The other state parameters include the initial anisotropy α_0 (calculated from the slope of the critical state line in compression) and the initial amount of bonding χ_0 (estimated based on sensitivity). A short explanation of how the parameters are evaluated, and for certain parameters their relation to the Swedish standard parameters is discussed in the following.

The modified swelling index κ^* is defined as the slope of the overconsolidated part of the stress-strain curve, i.e the unloading/reloading part of the compression curve in a ln(p')-ε_v-plot, and is usually estimated from an oedometer test. The modified intrinsic compression index λ_i^*, is defined in similar manner, but is associated to the (post yield) virgin loading curve. Since λ_i^* is an intrinsic parameter, it relates to the state when all apparent bonding has been destroyed.

Table 4.1: Layering of the model and the selected soil model.

Layer	Soil model	Depth [m]
Embankment	Mohr-Coulomb	2.9 to 0
Dry crust	Mohr-Coulomb	0 to -2
Soft Clay 1	Creep-SCLAY1S	-2 to -4
Soft Clay 2	Creep-SCLAY1S	-4 to -6
Soft Clay 3	Creep-SCLAY1S	-6 to -10
Soft Clay 4	Creep-SCLAY1S	-10 to -13
Soft Clay 5	Creep-SCLAY1S	-13 to -20
Friction material	Mohr-Coulomb	-20 to -25

Table 4.2: List of Creep-SCLAY1S parameters

κ^*	Modified swelling index
ν'	Poisson's ratio
λ_i^*	Modified intrinsic compression index
M_c	Slope of critical state line in compression
M_e	Slope of critical state line in extension
ω	Absolute effectiveness of rotational hardening
ω_d	Relative effectiveness if rotational hardening
ξ	Absolute rate of destructuration
ξ_d	Relative rate of destructuration
μ_i^*	Modified intrinsic creep index
τ	Reference time
POP	Pre overburden pressure (or alternatively OCR)
χ_0	Initial amount of bonding
α_0	Initial inclination of ICS, CSS and NCS

Thus, it needs to be evaluated from either a step-wise oedometer test on a remoulded clay sample, or from an oedometer test on a natural clay sample with very high stress level in the last loading steps, so that all the apparent bonding in the clay is destroyed. Equally to IL tests, results from CRS tested could be used, provided the sample can be loaded to high stress level. Usually, CRS tests are stopped well before that. Both κ^* and λ_i^* are calculated with Equation 4.1.

$$\kappa^*, \lambda_i^* = \frac{\Delta\varepsilon}{\Delta ln(p')} \tag{4.1}$$

where p is the mean effective stress.

It should be noted that κ^* and λ_i^* can be also be related to the confined modulus M_0 and the oedometer modulus number M', respectively, that are evaluated from CRS tests used in Sweden. The bonding parameters of the model are basically used to predict M_L, the confined modulus post-yield that is used as input for settlement analyses in Sweden. If for the sake of simplification the effects of apparent bonding are ignored, by switching the apparent bonding χ_0 to zero, the value for λ_i^* can be replaced by the modified compression index λ^* related to M_L. The relation between κ^*, λ_i^*, M_0 and M' are shown in Equations 4.2a, 4.2b and 4.2c. For

the relationships between other stress-strain parameters see (Olsson 2010).

$$\kappa^* \approx \frac{2 \cdot \sigma'_{vc}}{M_0} \tag{4.2a}$$

$$\lambda_i^* \approx \frac{1}{M'} \tag{4.2b}$$

$$\lambda^* \approx \frac{1.1 \cdot \sigma'_c}{M_L} \tag{4.2c}$$

σ'_{vc} in equation 4.2a is the average between the in situ vertical effective stress and the preconsolidation pressure σ_c.

The modified intrinsic creep index is an improtant parameter that controls, together with overconsolidation ratio (ORC), the creep are. If the modified creep index μ_i^* is calculated from Creep number (r or R), Creep index (C_{ae}) or Creep parameter (α_s), it is important to appreciate that μ_i^* is an intrinsic value. So, just like the modified intrinsic compression index λ_i^*, it needs to be evaluated from a step-wise oedometer test (IL) on a remoulded clay sample or from volumetric strain vs. $ln(time)$ plot of a stage at very high stress in an oedometer test. An overly high creep index, such as the value just after the preconsolidation pressure is exceeded, can lead to unrealistically high creep rates that can cause problems in the FE model. For example, with too high value for μ_i^*, the process of creep can continuously generate excess pore pressures instead of allowing them to dissipate, or alternatively unrealistically large background creep deformations are predicted. (By background creep deformations we mean creep strains predicted with in situ stresses only, without loading the soil e.g. without the embankment in our case).

The initial value for the initial bonding parameter χ_0 can be estimated from sensitivity S_t by Equation 4.3:

$$\chi_0 \approx S_t - 1 \tag{4.3}$$

Further calibration of χ_0 is done by simulation of the oedometer tests, but generally it is the order of magnitude that matters. The more sensitive and structured a clay is, the more "brittle" the soil appears (i.e. only a small increment of vertical effective stress is required to compress a sample to a certain strain). A highly sensitive (quick) clay with a sensitivity over 50, might only need a load between 300 to 500 kPa to reach a vertical strain of 30%. A non-sensitive to slightly sensitive clay (sensitivity $S_t < 10$) might require a load at least twice of that to reach the same magnitude for the vertical strain.

The slope of the critical state line M_c (and thus the critical state friction angle) was evaluated from triaxial compression tests, which in case of Haarajoki involved both drained and undrained triaxial compression tests. As there were no triaxial extension tests available for Haarajoki clay, the slope of the critical state line M_e in extension was calculated with Equation 4.4, assuming a failure in extension according to the Mohr Coulomb model prediction:

$$M_e = \frac{3M_c}{(6 - M_c)} \tag{4.4}$$

The earth pressure coefficient at rest for normally consolidated soil K_0^{nc} was calculated with Jaky's formula (Jaky 1948). This coefficient is used to estimate the stress ratio η_{K0} for 1D normally consolidated loading, needed to calculate the model parameters for initial anisotropy

α_0 and the relative effectiveness of irrecoverable volumetric and shear strains in rotating the model surfaces, i.e. ω_d. The initial anisotropy α_0 is calculated with Equation 4.5 that is theoretically derived from the model, as explained in Wheeler et al. (2003). It applies to a deposit that is either normally consolidated or lightly overconsolidated with K0 (1D) loading history, with horizontal soil layers.

$$\alpha_0 = \alpha_{K0} = \frac{\eta_{K0}^2 + 3\eta_{K0} - M^2}{3} \tag{4.5}$$

Similarly, based on theoretical considerations, ω_d can be calculated with the following equation (Wheeler et al. 2003):

$$\omega_d = \frac{3(4M^2 - 4\eta_{K0}^2 - 3\eta_{K0})}{8(\eta_{K0}^2 - M^2 + \eta_{K0})} \tag{4.6}$$

The model parameters ξ and ξ_d, relating to destructuration, can be determined by very specific drained triaxial tests: one involving isotropic loading (for ξ) and one involving radial loading with a high stress ratio (for ξ_d) Koskinen et al. (2002). As those are usually not available, the values can be calibrated by simulation of oedometer tests. Gras et al. (2018) has suggested both a theoretical lower and upper bound for ξ. Usual values are between 9 and 14 for ξ and 0.2 to 0.4 for ξ_d.

The initial value for the absolute effectiveness of rotational hardening ω can be estimated by Equation 4.7 (Leoni et al. 2008). The value of ω can be further calibrated by modelling an undrained triaxial extension test that has been consolidated anisotropically to in situ stress level, and comparing the results with experimental data. ω namely has a major effect of the predicted stress path (and thus pore pressures) during undrained shearing the triaxial extension. Unfortunately for Haarajoki test embankment, no triaxial extension results are available.

$$\omega = \frac{1}{(\lambda_i^* - \kappa^*)} ln\left(\frac{10M_c^2 + 2\alpha_{K0}\omega_d}{M_c^2 + 2\alpha_{K0}\omega_d}\right) \tag{4.7}$$

For Haarajoki test embankment, once initial values for all model parameters were derived, further calibrations of the parameters were done by modelling the available laboratory tests. These simulations were performed for step-wise oedometer tests and the triaxial compression tests. An example of these simulations, compared to the lab data can be seen in Figure 4.2. The final parameters used in the model are displayed in Table 4.3. The values for K_0 relate to the estimated in situ value of the earth pressure at rest, so strictly speaking it is not a model parameter, but needed to create representative horizontal effective stresses at the initialisation of stresses at the start of the analyses.

4.2 Parameters for Mohr-Coulomb model

The Mohr-Coulomb model is used for two soil layers, the dry crust and bottom moraine, as well as the embankment. Since it is the soft clay deposits that is the focus of this analysis, it has been assumed that any deformations that occur in the friction material, dry crust and the embankment itself are negligible. For this reason, a very high stiffness has been assumed for the friction material and the embankment. The stiffness of dry crust is set to represent the stiffness of a stiff overconsolidated clay. All parameters used in the Mohr-Coulomb materials are shown in Table 4.4.

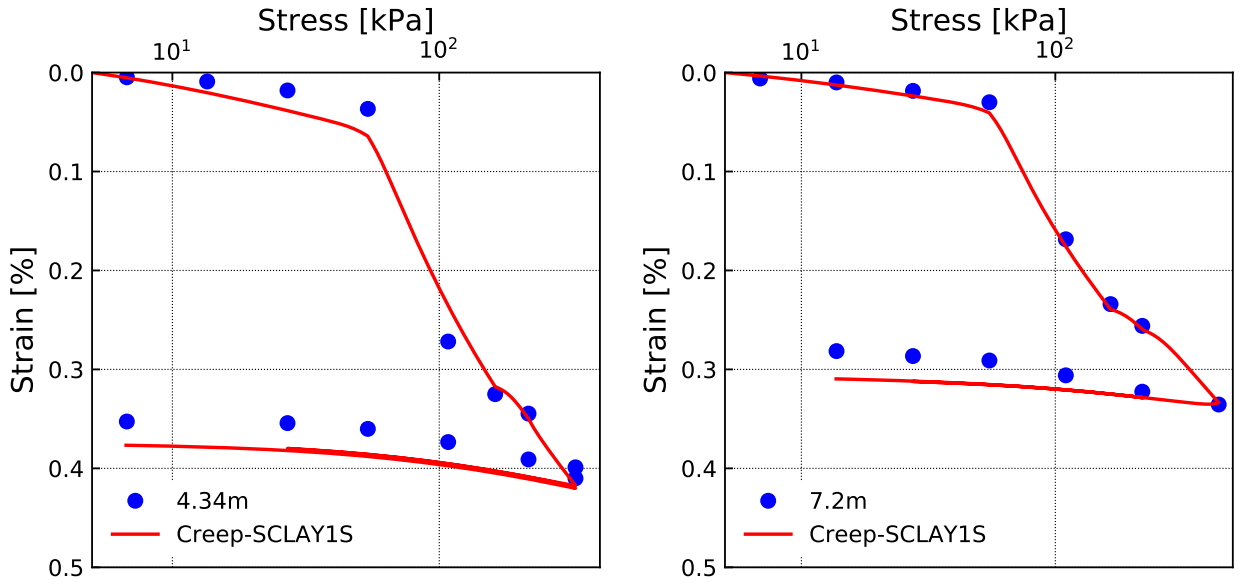

(a) (b)

Figure 4.2: *Step-wise oedometer tests from 4.34 (a) and 7.2 (b) meters depth and simulation of them with Creep-SCLAY1S.*

Table 4.4: Parameters for the Mohr-Coulomb model.

Parameters	Dry Crust	Friction material	Embankment
Unit weight γ, (kN/m^2)	17	19	20
Young's modulus E', (kN/m^2)	4077	40000	40000
Poisson's ratio ν'	0.2	0.2	0.35
Cohesion intercept c_{ref}, (kN/m^2)	20	2	2
Friction angle ϕ, (°)	5	40	40
Earth pressure at rest in situ, K_0	0.91	0.36	0.36
Hydraulic conductivity k, (m/day)	1.30E-03	1	1

4.3 Other parameters

The hydraulic conductivity k is typically not equal in the vertical and horizontal direction for natural soft clay layers. In the case of Haarajoki, the hydraulic conductivity is higher in the horizontal direction than the vertical direction for all soft clay layers based on the oedometer tests. Changes in the hydraulic conductivity during consolidation is modelled by the hydraulic conductivity change index C_k, which was assumed to be equal to $0.5e_0$ as been suggested by Tavenas et al. (1983). The hydraulic conductivity change index C_k is assumed to be the same for both the vertical and horizontal direction. All values used for the hydraulic conductivity and hydraulic conductivity change index are shown in Table 4.5.

Table 4.3: Parameters used for Creep-SCLAY1S to model the five soft clay layers.

Parameters	Layer 1	Layer 2	Layer 3	Layer 4	Layer 5
γ, (kN/m^3)	13.8	14.2	15.0	15.0	16.0
κ^*	0.0065	0.0088	0.0075	0.0100	0.0170
ν'	0.2	0.2	0.2	0.2	0.2
λ_i^*	0.108	0.100	0.084	0.084	0.087
M_c	1.15	1.15	1.20	1.20	1.50
M_e	0.83	0.83	0.86	0.86	1.00
ω	24	35	20	20	20
ω_d	0.144	0.622	0.600	0.600	0.600
ξ	9	9	12	12	9
ξ_d	0.20	0.22	0.25	0.25	0.25
POP, (kPa)	50	40	35	35	25
e_0	3.30	3.00	2.40	2.40	1.96
α_0	0.43	0.45	0.46	0.46	0.46
χ_0	10	10	15	20	25
τ, (days)	1	1	1	1	1
μ_i^*	0.003	0.004	0.002	0.002	0.001
K_0	0.68	0.68	0.61	0.61	0.76

Table 4.5: The vertical k_v, horizontal k_h hydraulic conductivity and the hydraulic conductivity change index C_k.

Layer	k_h [m/day]	k_v [m/day]	C_k
Dry crust	0.0013	0.0013	-
Soft clay 1	1.56E-04	1.30E-04	1.65
Soft clay 2	1.56E-04	1.30E-04	1.5
Soft clay 3	1.38E-04	6.90E-05	1.26
Soft clay 4	1.30E-04	6.50E-05	1.26
Soft clay 5	8.00E-04	1.12E-04	0.98
Friction material	1	1	-

5 Results

5.1 Reference case: Haarajoki test embankment

For the reference case the section of Haarajoki test embankment without the drains has been modelled as a 2D time-dependent analysis. The embankment was modelled until 90% of the excess pore pressure generated by the construction had dissipated, which took 38000 days or 104 years after the embankment was completed. At this point the majority of the primary consolidation was deemed to be completed. Based on the analyses, the final settlement is expected to be about 1.4-1.5 m, i.e. about the half of the embankment height.

The model captures the settlements under the centre line very well, when compared to the available measured settlements. This is displayed in normal and semi-log scale in Figure 5.1a and 5.1b, respectively. Of course, it is still possible that the predicted time-settlement curve start to diverge later on from the measurements. The latest available settlement measurements is suggesting that the degree of consolidation (based on settlement rate) after about 10 years of consolidation is just over 40%. However, the fact that we are also able to make decent predictions with the model for the vertically drained section Amavasai et al. 2017, which consolidates much faster, gives us some additional confidence in our ability to predict the settlement rate.

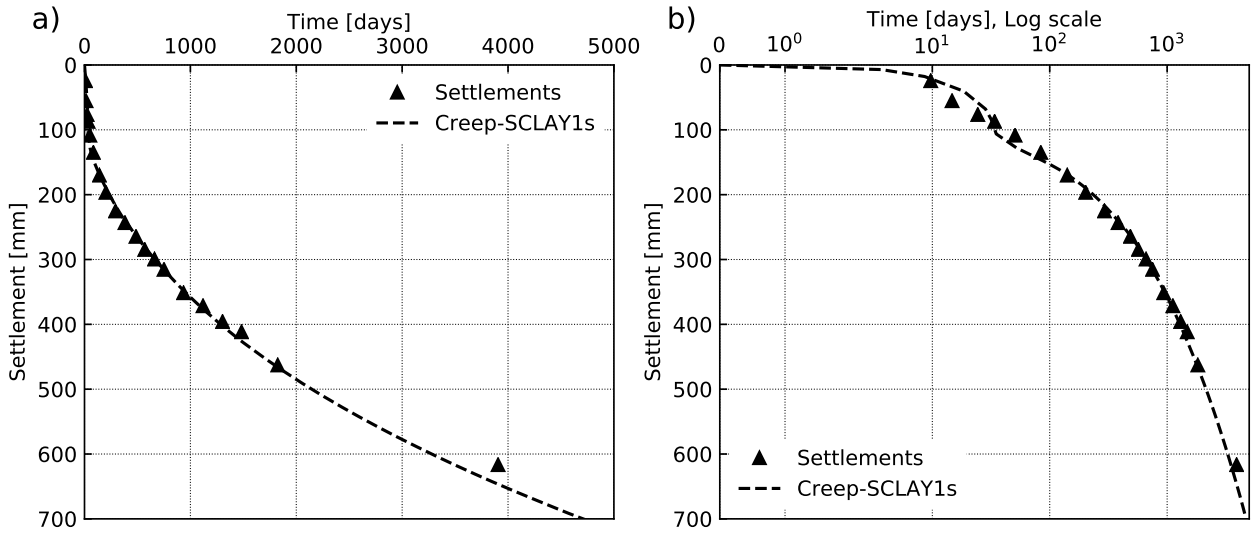

Figure 5.1: *(a) Measured and modelled settlement in the centre line as a function of time. (b) Measured and modelled settlement in semi-log scale.*

The pore pressure development under the embankment was modelled reasonably well, see Figure 5.2. The maximum excess pore pressure predicted by the model was 30 kPa, at a depth of five meters beneath the original ground surface. These results were comparable with the available field measurements from the piezometers, which is shown in Figure 5.2a using solid symbols. The model was able to predict the maximum value of the excess pore pressure reasonably well, but the measured maximum is deeper down, as shown in Figure 5.2b. The measured value of the excess pore pressure at four meters depth was lower than predicted by the model and lacked a clear peak. This indicates that the hydraulic conductivity of the

first clay layer probably is higher than the one used in the model, or that the vertical drains installed to the other section of the embankment could influence the results. Alternatively, we are simply underestimating the stiffness in the first soft clay layer. At 15 meters depth the model underestimated the peak value of excess pore pressure. However, the long term trends of the excess pore pressure was captured reasonably well at all depths. Previously published simulations with simpler (non-creep) models (Yildiz et al. 2009) were unable to capture the pore pressure response as well as Creep-SLAY1S.

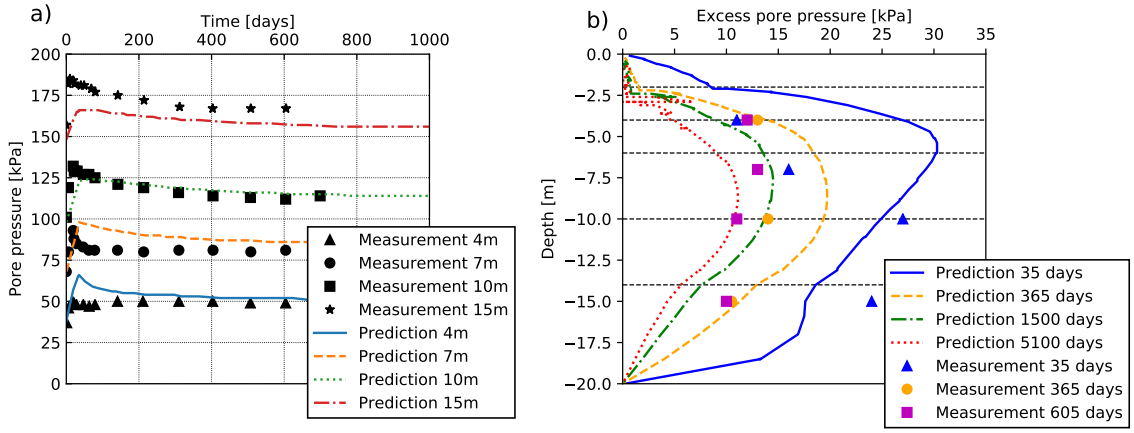

Figure 5.2: *(a) Pore pressure measurements and model results at 4, 7, 10 and 15 meters depth. (b) Predicted excess pore pressure against depth after 35, 365, 1500 and 5100 days.*

Figure 5.3 shows the measured and predicted horizontal displacements under the toe of the embankment against depth. Overall, the model overpredicts the measured horizontal displacements. The predicted horizontal displacements also goes deeper in the clay deposit than the measured horizontal displacements. Given the settlements of this section appear to be affected by the section with vertical drains (Lojander and Vepsäläinen 2001), it is also possible that by matching the vertical settlements we are actually overpredicting them, and correspondingly overpredicting the horizontal movements. However, we also need to appreciate that given there were no triaxial tests in extension, we are unable to properly calibrate ω that governs the rotation of the compression surfaces, i.e. evolution of anisotropy, which will affect the prediction of horizontal displacements. Finally, there were problems with the inclinometer measurements in Haarajoki, with measurement under the crest of the embankment having a lot of noise (and thus not included in comparisons here) and the readings were unfortunately stopped after 1090 days.

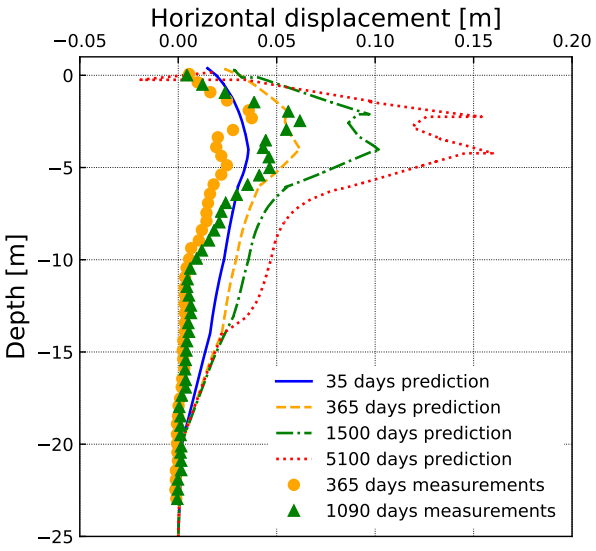

Figure 5.3: *Predicted and measured horizontal displacements against depth below the toe of the embankment after: 35, 365, 1090, 1500 & 5100 days.*

As the purpose of the simulations is to investigate the evolution of undrained shear strength, the next question is how well the model can predict the apparent s_u prior to embankment construction. In the finite element analyses with an effective stress model, the undrained shear strength s_u is not a direct input, but a result of the model prediction for a given stress path, starting from a given effective stress state. It is thus important to check that the s_u value resulting from the model corresponds to the measured s_u values. The initial s_u predicted with the model for a direct simple shear test v(which we assume to be closest the the field vane test) versus the field vane test can be seen in Figure 5.4. The predictions are very good from 5 m depth downwards, even if one needs to be careful when comparing the results between different types of tests, also done at different strain rates. There are no DSS test results available, however those are not particularly useful, given we have do not know the horizontal effective stresses in a DSS test. Clearly, we are also underpredicting the s_u just under the dry crust, i.e. the first soft clay layer.

The initial equivalent E modulus for in Figure 5.4 is simply estimated using elasticity theory given the deposit is overconsolidated. In Creep-SCLAY1S the value of Poisson's ratio ν' is assumed to be constant, and thus the bulk modulus K can be calculated with κ^* and p', the mean effective stress. With K and ν' known, the initial E modulus then be calculated with Equation 5.1.

$$E = 3K(1 - 2\nu) \tag{5.1}$$

Attempts to bring the embankment to failure were not successful using gravity loading in Plaxis. Thus, the values in Figure 5.4 are subsequently used as an input for a stability analysis of the embankment with Finite Element Limit Analysis (FELA) in Optum G2 (Optum G2 2020), which calculates Factor of Safety (FOS) for the lower and upper bound of the limit state problem. The results are sensitive to the s_u values assumed for the dry crust. Thus, depending on the s_u chosen for the dry crust the FOS varies between about 1.237 and 1.473, as shown in

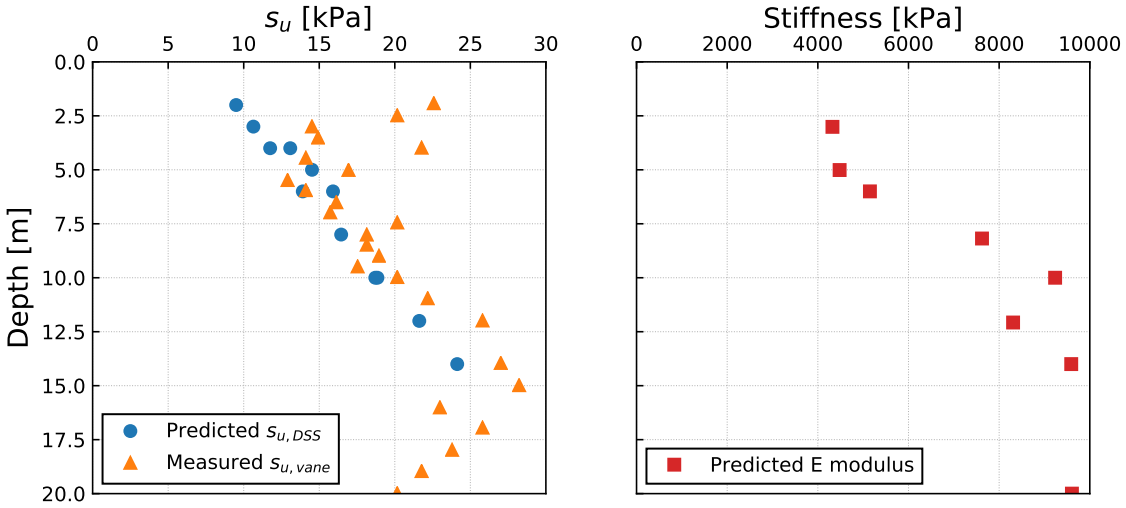

Figure 5.4: *The initial s_u (from field vane and predicted by Creep-SCLAY1S for DSS), on left, and the initial stiffness predicted with the model, on right.*

Table 5.1. The lower and upper bound failure mechanisms are shown in Figures 5.5a and 5.5b. These results corresponds quite well with the factor of safety aimed for in the design of the test embankment, which was a FOS of 1.3. Based on this, the selected set of model parameters appears to give reasonably realistic prediction of both the stress-strain response as a function of time, as well as the distribution of the initial undrained shear strength s_u.

Table 5.1: Factor of safety of Haarajoki test embankment evaluated with predicted initial s_u with Finite Element Limit Analysis (FELA).

	Factor of Safety		
s_u Dry crust	Lower	Upper	Mean
10 kPa	1.221	1.252	1.237
15 kPa	1.361	1.392	1.377
20 kPa	1.453	1.493	1.473

Since the predictions by the model seem to have captured the overall response of the clay deposits reasonably well, the data required for the element level simulations was extracted from the simulation results. Data was extracted from several depths below the centreline of the embankment. The centreline was chosen to avoid issues with the rotation of the principal stress axes. As demonstrated in Figure 5.6, at the toes of the embankment the principal stress direction can be rotated by close to 90° in the top layers of the soil deposit.

Figure 5.7a and Figure 5.8a show how the Cartesian components of the effective stress tensor are predicted to change with time under the centreline of the embankment. Figure 5.7a illustrates that there is no stress rotation, since the shear stress component σ_{xy} remains at zero. In the case of plane strain analyses, the components of the horizontal effective stress are of course not equal, thus we no longer have triaxial stress conditions. In contrast, under the toe of the embankment in Figure 5.8a, a shear stress component in excess of 10 kPa is predicted to develop after construction of the embankment, demonstrating (as expected) that

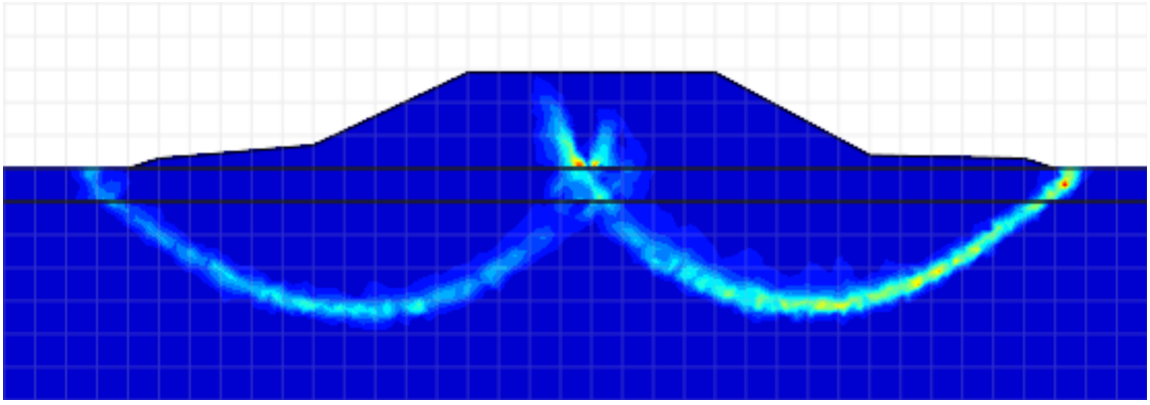

(a) *Lower bound.*

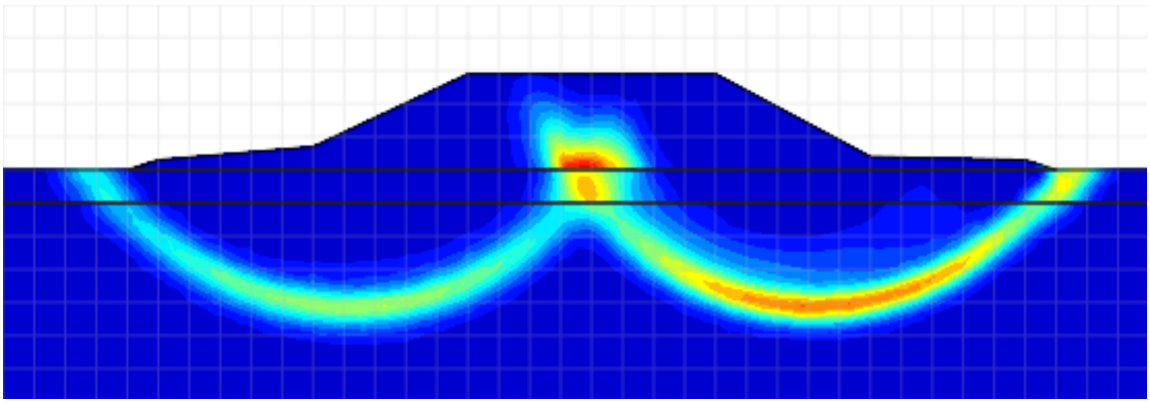

(b) *Upper bound.*

Figure 5.5: *Predicted failure mechanism with FELA.*

there is significant stress rotation. For this reason alone, there is no point in taking samples underneath the slope if the gain of the undrained shear strength is experimentally investigated, as the main axes of the effective stresses of the sample will not coincide with the main axes in the test apparatus.

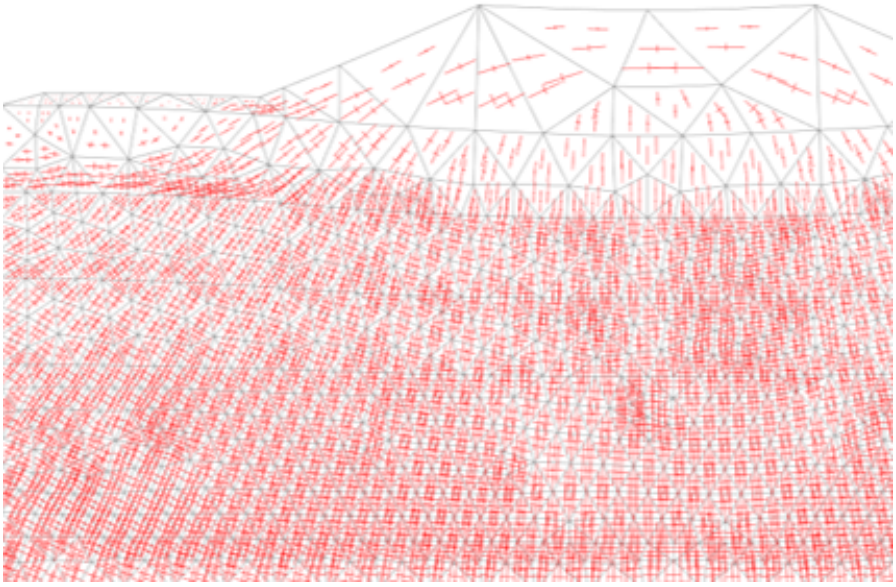

Figure 5.6: *Direction of principal stress under the embankment.*

The situation is very similar with regards to the evolution of anisotropy, represented by the components of the fabric tensor. Under the centreline in Figure 5.7b, there is no notable change in anisotropy after application of the embankment load, as the components of the fabric tensor and the scalar value of α remain constant. This is what would be expected, if the deposit had had a K_0 deposition history. Under the toe in Figure 5.8, in contrast, there is significant evolution of anisotropy (rotation of the model surfaces), which can most clearly be illustrated by the changes in the α_{xy} component (fabric distortion). Initially the dominating direction for the a fabric is vertical and the radial components are equal ($\alpha_y y$ ¿ $\alpha_x x{=}\alpha_z z$), due to the K_0 deposition history. As a function of time, the anisotropy is evolving, with $\alpha_y y$ reducing and $\alpha_x x$ increasing. Furthermore, due to the plane strain condition, $\alpha_x x$ and $\alpha_z z$ diverge. Consequently, any sample taken under the slope of an embankment would have a complex initial stress and fabric state.

This effective stress and fabric rotation would need to be taken into account when performing laboratory tests for soil samples taken under the slopes of the embankment. As for modelling, the soil sample would need to be simulated in 3D with boundary conditions that apply to the particular test. Furthermore, if such a sample is tested e.g. in a triaxial cell, it is expected to deform non-uniformly in the radial direction and thus, the shape of the sample would need to be measured throughout the test. Since this is not particularly practical, it was decided to focus on the centre line.

A test embankment is usually a plane strain problem, and thus the effective stresses in the out of plane direction are not the same as in the horizontal direction. Because the soil is not able to move in the out of plane direction, the effective stress increase is higher in out of plane than the in-plane horizontal effective stress. The out of plane dimension is not properly taken into account in an ordinary triaxial test. To do this it would be necessary to perform a true triaxial test, which means controlling the stresses and strains in all three dimensions on a cubical sample. Since true triaxial tests are not regularly performed, for this project the difference was explored numerically in a strain driver, to quantify the difference between the standard triaxial test and the true triaxial test. The results are shown in Figure 5.9a and 5.9b. In the initial situation (black lines), there is of course no difference as $\sigma'_2{=}\sigma'_z z$ and $\sigma'_3{=}\sigma'_x x$,

see are equal. Because the soil is overconsolidated to start with, the stress path goes initially straight-up, reflecting an almost purely elastic response, and hits the Normal Consolidation Surface on the left side on the critical state line, resulting in a stress path that veers towards right, with small strain softening at the end of the simulation. After 5100 days of consolidation, the starting stress states in the triaxial and true triaxial differ, as due to the plane strain condition σ'_2 ¿ σ'_3. This difference increases with time.

The results show that there is a difference in the predicted undrained shear strength s_u between the ordinary and true triaxial simulation, especially for the shallow layer, see Figure 5.9a. The deviator stress at failure in triaxial conditions is of course linked with the predicted s_u=q/2. Overall, the predicted deviator stress at failure is higher for ordinary triaxial than the true triaxial. The difference is though only a few kPa.

Importantly, this difference in peak s_u decreases and basically disappears with depth. At 5.5 meters depth, the starting point of the stress path differs of course slightly due to consolidation in plane strain condition, but the predicted peak s_u values from the true and ordinary triaxial were practically equal as shown in Figure 5.9b. The difference in peak s_u between the ordinary and true triaxial thus decreases with depth, as the horizontal stresses σ'_2 and σ'_3 are similar.

The analyses looking at how the s_u values are predicted to change as a function of time was focused on the two first clay layers directly under the dry crust, where the majority of the volumetric deformations were predicted, as shown in Figure 5.10. Data was extracted from stress points at the following depths from the original ground surface, i.e. 2.4, 3, 3.6, 4.1, 4.6, 5 and 5.5 m. These stress points were then analysed at the following time steps: directly after construction of the embankment, one year, four years, 14 years and after 90% dissipation of the excess pore pressure (which corresponds to 104 years in this case).

The element level simulations were done for the selected stress points in clay layers one, two and in the middle of the third. The results for these simulations are displayed in Figure 5.11 and Figure 5.12. Both figures show the predicted s_u normalised with the initial s_{u0} for each depth, and the peak s_u value for the three element level tests, i.e. triaxial compression, triaxial extension and direct simple shear, at each time step of interest.

The undrained shear strength s_u is predicted to increase at all depths. However, the increase was smaller in Clay layer 1 than Clay layer 2, and there was only a marginal increase predicted in the deeper clay layers of the deposit. This is consistent with what can be seen in Figure 5.10, where the largest volumetric strains are located in the second clay layer. Furthermore, this is consistent with the results in (Vepsäläinen et al. 2002), which despite the significant (excess of 400 mm) settlement, indicated modest gains in the s_u values and other relevant parameters, such was water content, even when the depth coordinates of the latter were corrected for the settlements (based on numerical analyses).

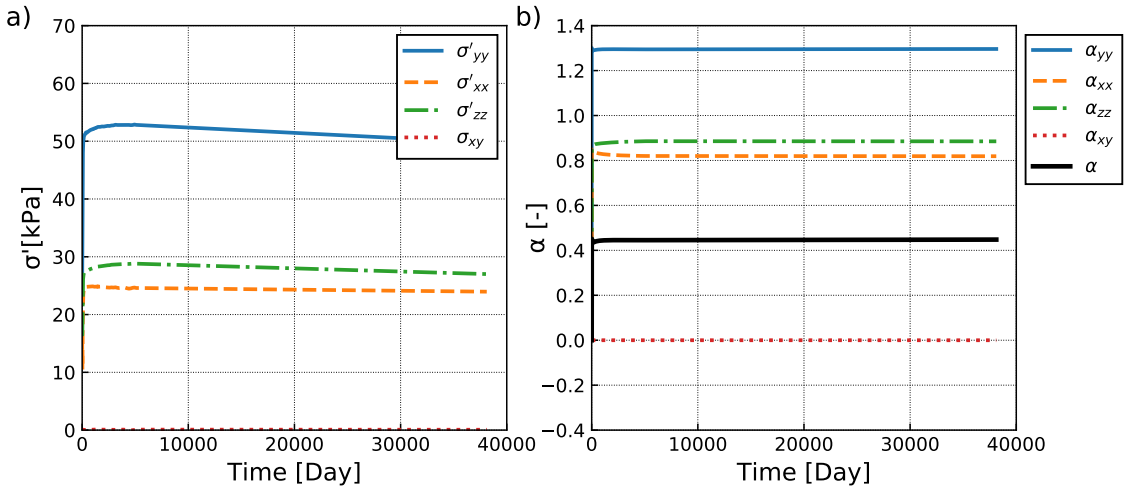

Figure 5.7: *At 4.1 meters depth under the centreline of the embankment. Predicted changes in (a) effective stress tensor and (b) fabric tensor.*

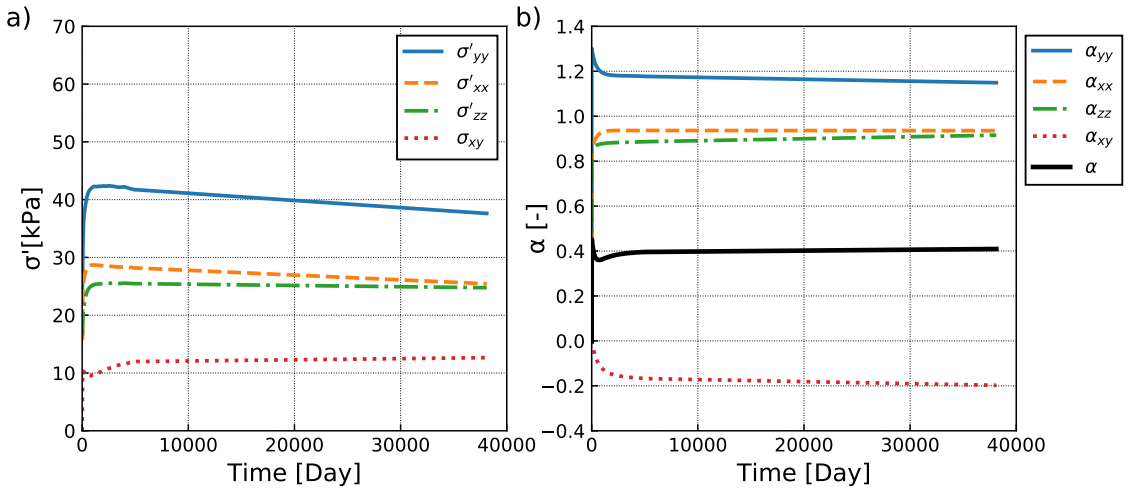

Figure 5.8: *At 4.1 meters depth under the toe of the embankment. Predicted changes in (a) effective stress tensor and (b) fabric tensor.*

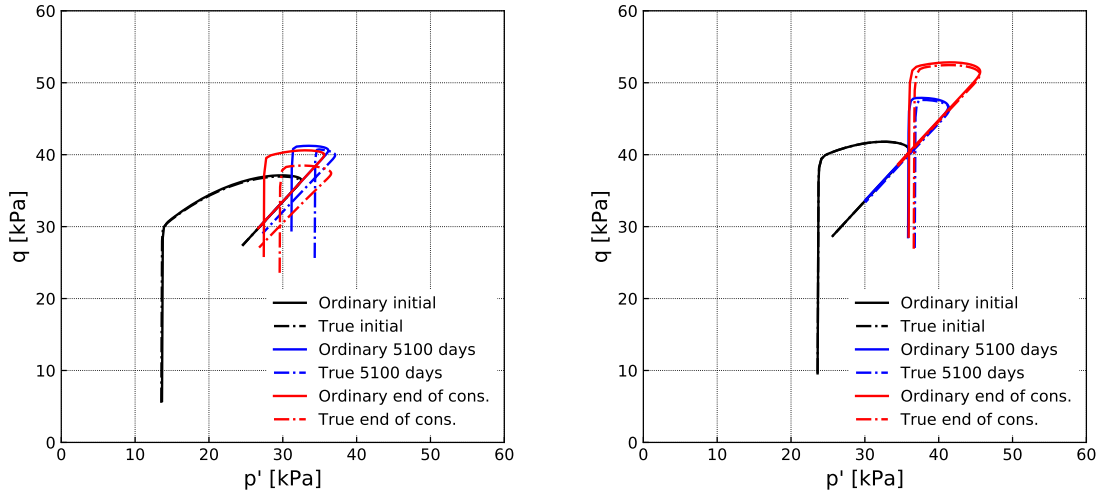

Figure 5.9: *Predicted stress path for the ordinary triaxial and the true triaxial test (a) 2.4 meters depth, (b) 5.5 meters depth.*

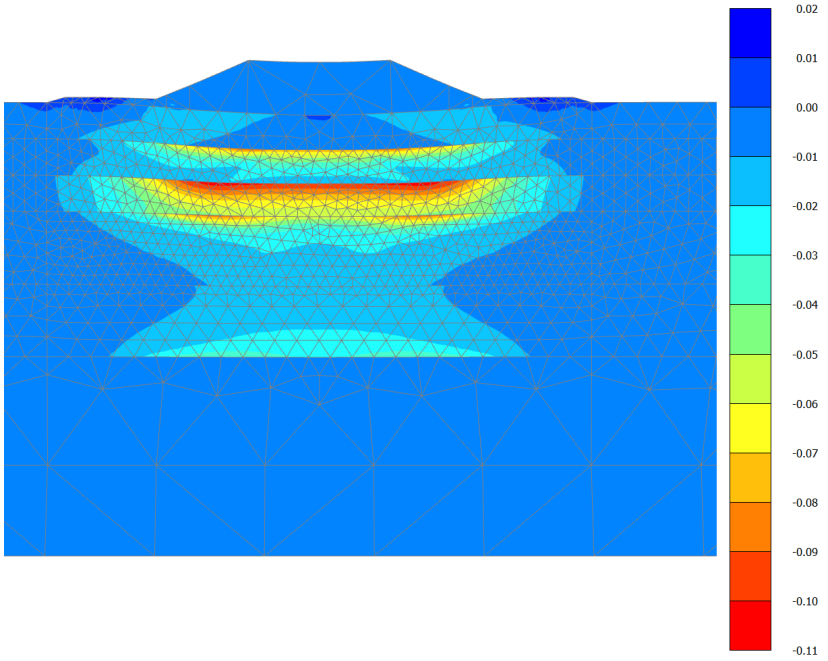

Figure 5.10: *Volumetric strain (%) distribution after 5100 days of consolidation.*

In the first clay layer (depths 2.4, 3 and 3.6 m), the predicted changes in s_u were quite small, at most about 15% and in most cases less than that. This can be seen in Figure 5.11a to 5.11f. The reason for this is most likely the high preconsolidation pressure in this part of the deposit. Furthermore, the predicted (excessively) large horizontal displacements reduce the effective stress, which probably also prevents larger increases in s_u. Most of the gain is predicted to occur very early on, thus dominated by shear strains.

The second clay layer (depths 4.1,4,2,5 and 5.5m) is predicted to have an increase of s_u of 25% to 30%, as is shown in Figure 5.11g-h and 5.12a-f, increasing with time. In absolute terms this is equal to 5 to 6 kPa in compression, 3 to 4 kPa in direct simple shear and 2 to 3 kPa in extension. The second layer seems to be located sufficiently deep to avoid any decrease in effective stress due to the horizontal movements. This small increase does not in practice increase the FOS, except marginally.

In the middle of the third layer (depth 8 m), the predicted changes in s_u were small compared to layer one and two, in percentage around 10% and between 1 and 3 kPa in absolute terms as shown in Figure 5.12g and 5.12h after primary consolidation has finished. Such small changes are not surprising since the volumetric strains are less than 3% for most of the layer. This again is most probably due the fact that the preconsolidation pressure σ'_c was not exceeded.

Most importantly, Figure 5.11 show that the increase in the mobilised undrained shear strength in the different directions is not the same in the top layers. At 3 m depth, see Figure 5.11c, the undrained shear strength is actually predicted to be reducing in time, and in particular for triaxial extension predicted to be lower than it was initially. In contrast, in deeper layers, see Figure 5.12, the undrained shear strength is predicted to increase in time, and the increase is predicted to be the same in all directions. The results, even though inconclusive hint that the increase in the undrained shear strength does not always guaranteed, in particular if we do not exceed the preconsolidation pressure and/or predicts excessive horizontal deformations displacements.

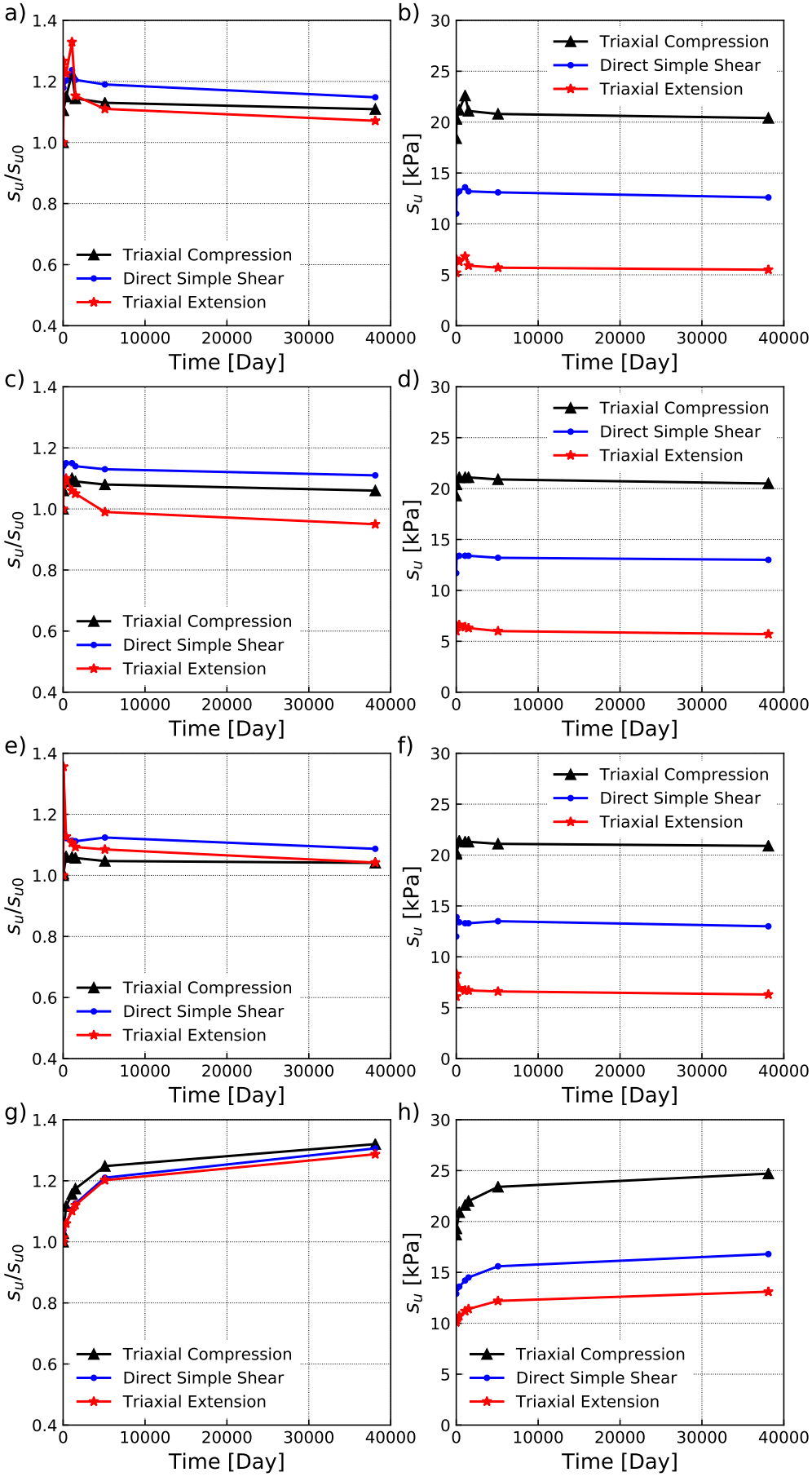

Figure 5.11: *Normalised s_u/s_{u0} and peak s_u for the depths : 2.4 m (a-b), 3 m (c-d), 3.6 m (e-f) and 4.1 m (g-h) meters depth.*

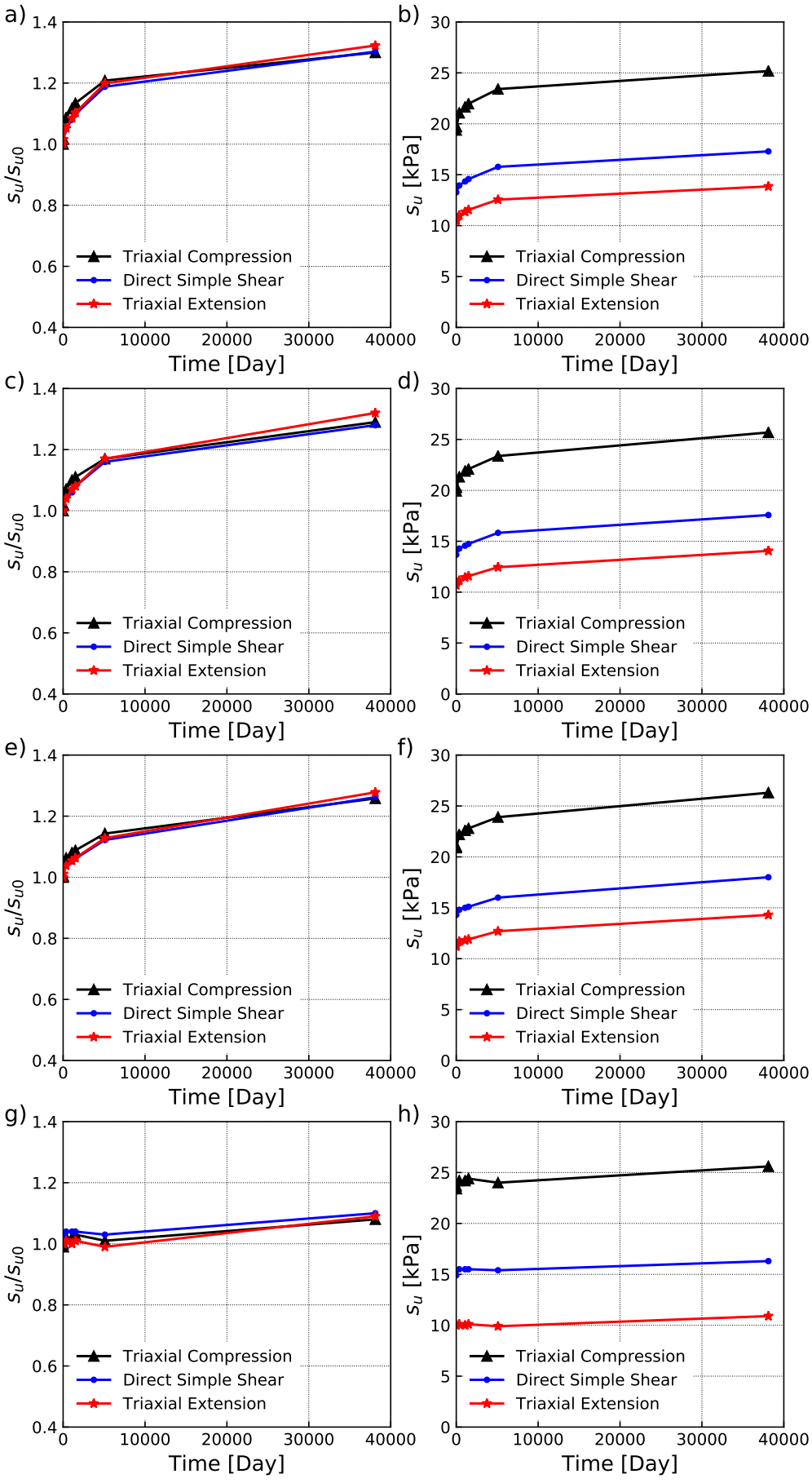

Figure 5.12: *Normalised s_u/s_{u0} and peak s_u for the depths: 4.6 m (a-b), 5 m (c-d), 5.5 m (e-f) and 8 m (g-h).*

5.2 Sensitivity analyses

Sensitivity analyses were performed to study the influence of certain model parameters on the predicted response. The model parameters that were altered in the analyses were the intrinsic creep index μ_i^* and the pre-overburden pressure (POP). POP, or rather the apparent preconsolidation pressure controls both primary consolidation and creep rate, whilst μ_i^* controls the "pure creep" rate in the formulation of Creep-SCLAY1S (Gras et al. 2018). Thus, relatively small changes in the values of these parameters can have rather large effect on the results.

Three different analyses were done. In one of the simulation POP was increased by 20 kPa, which correspond to the case when the groundwater level is 2 m below the surface, as it has been sometime in the past, given the thickness of the dry crust. In order to assess the role of "pure creep", the initial values of μ_i^* have been multiplied by 2 and divided by two. Once again, the model simulations were terminated once 90% of the generated excess pore pressure had dissipated. Thus, how long the primary consolidation took varied between the different cases, see Figure 5.13aa. The changes in the parameters above influenced the extent/depth of the deposits that was affected by the embankment, see Figure 5.13ab, even though the embankment geometry was kept the same. For this reason, an additional level in the third layer was analysed. The effects on the deeper parts of the deposits were still marginal in all additional three cases studied in the sensitivity analysis.

The settlement against time curves of the different cases are shown in Figure 5.13a. As already discussed, the changes in the parameter values affect both the magnitude of the final settlement, and the time required to reach the final settlement. The results show that both adjusting the creep parameter and reducing the overconsolidation (POP) have a major effect on the predicted settlements. Figure 5.13b shows the predicted vertical displacements against depth at the end of primary consolidation. The zigzagging curves for the cases $\mu_i^* \cdot 2$ and POP -20 are due to local numerical instabilities. The predicted horizontal displacements at the toe of the embankment for the four cases after 1500 days and the end of primary consolidation, are displayed in Figure 5.14a and 5.14b. The horizontal displacements at the end of consolidation appear to be somewhat proportional to the vertical displacement for these cases.

In the first case, the value for the creep parameter μ_i^* was multiplied by 2, increasing the creep rate. It is predicted to take about 150 years until 90% of the excess pore pressure had dissipated, which is about 50 years longer than in the reference case. Thus, creep is delaying the consolidation by generating additional excess pore pressures, and furthermore, higher creep rate also results in a increase in the ratio of creep settlements vs. primary consolidation settlement.

Both the final settlements and the increase in the predicted s_u of the clay (see Figure 5.15) were larger than in the reference case. This again confirms that significant changes in volume (void ratio or the water content) are needed for significant increases in the mobilised undrained shear strength. Compared to the corresponding points in the reference case, the relative change in s_u was larger for all points in this case. The largest changes were still predicted in the second layer, where the s_u increased between 60% to 80%, as can be seen in Figure 5.15. At the corresponding points in the reference case the predicted the increase was around 30%. Again, in the top layers, some reduction in the mobilised shear strength is predicted as a function of time, while deeper down there is either increase or no change.

In the second case the intrinsic creep index μ_i^* was divided by two, reducing the creep rate. In this case it only took about 18000 days until 90% of the excess pore pressure had dissipated,

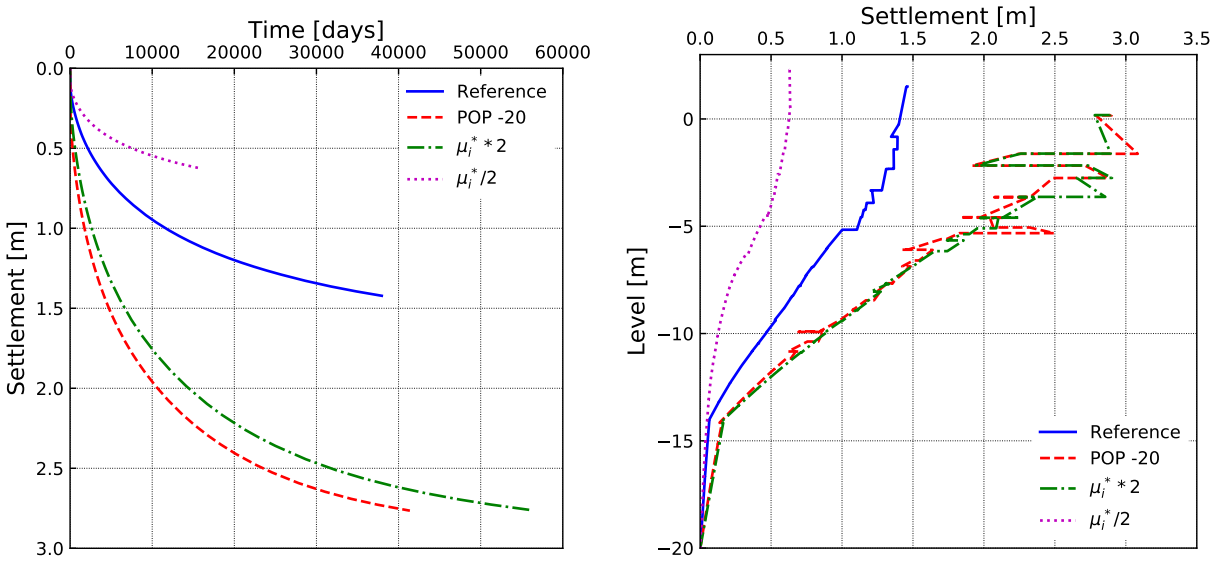

(a) (b)

Figure 5.13: *Predicted vertical settlements for sensitivity studies a) as a function of time; b) as a function of depth at the end of primary consolidation.*

which was less than half of the time of the reference case. The undrained shear strength s_u is predicted to increase, both for the triaxial compression and direct simple shear. However, compared to the reference case, the predicted final undrained shear strength changes were smaller. As can be seen in Figure 5.16 while the predicted increase wan between 10% to 20%, in the reference case was an increase between 10% and 30% was predicted. At 2.5, 3.5 and 9.5 meters depth the undrained shear strength remained either the same, or even decreased slightly.

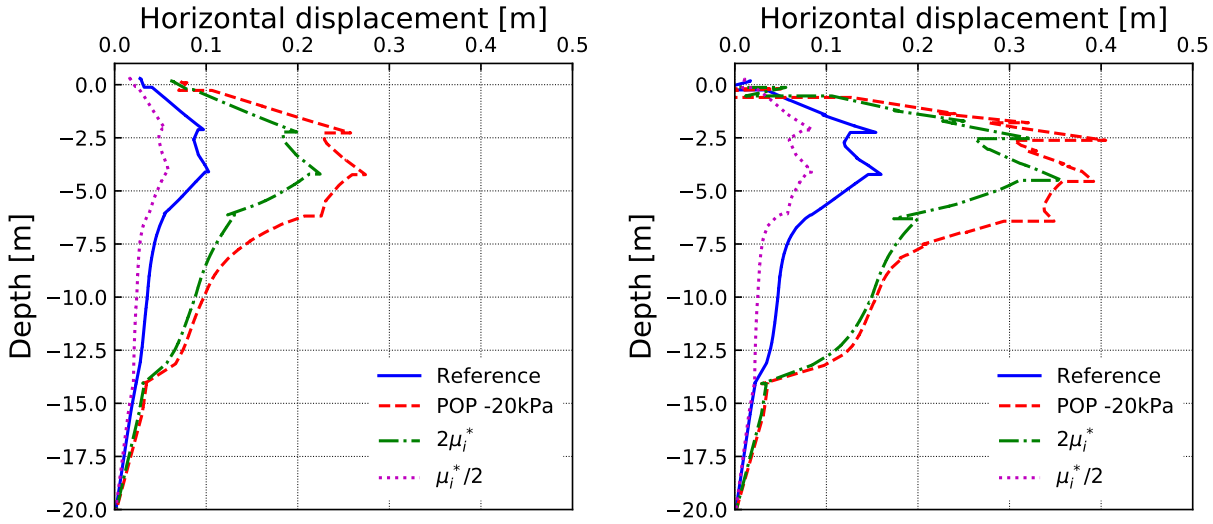

Figure 5.14: *Predicted horizontal displacements of the toe of the embankment a) after 1500 days and b) at the end of primary consolidation.*

In the third case the pre-overburden pressure was decreased with 20 kPa, corresponding to a situation when the groundwater level is just below the dry crust. Based on the model predictions, it takes a bit over 40000 days until 90% of the excess pore pressure had dissipated. This was only slightly longer than in the reference case. Together with the first two cases, in which the creep index was changed, this demonstrates the influence of the creep on the time frame of the dissipation of excess pore pressure in the model. The interdependence between consolidation and creep is complex: the creep effects are reflected in the consolidation response. The process of creep creates additional pore pressures when the volumetric strains are suppressed. This coupled with multidimensional consolidation can lead to increasing pore pressures for a long time after construction, as predicted and measured in Figure 5.2a. Thus, the undrained strength is not the lowest at the end of construction as suggested by 1D consolidation theory.

The predicted relative change in the undrained shear strength was larger at all depths compared to the reference case when POP was reduced. As can be seen in Figure 5.17, it is in the second layer that the biggest increase of undrained shear strength was predicted to occur. The increase was between 40% to 50%, consistent with the reference case where the largest relative increase also occurred in the second layer. It should also be noted that at 7.5 and 9.5 meters depth (Figure 5.17e and f), a slight decrease in the undrained shear strength after the construction of the embankment in predicted. This due to the excess pore pressures generated by the construction and undrained creep, which decrease the effective stress, before the excess pore pressures start to dissipate.

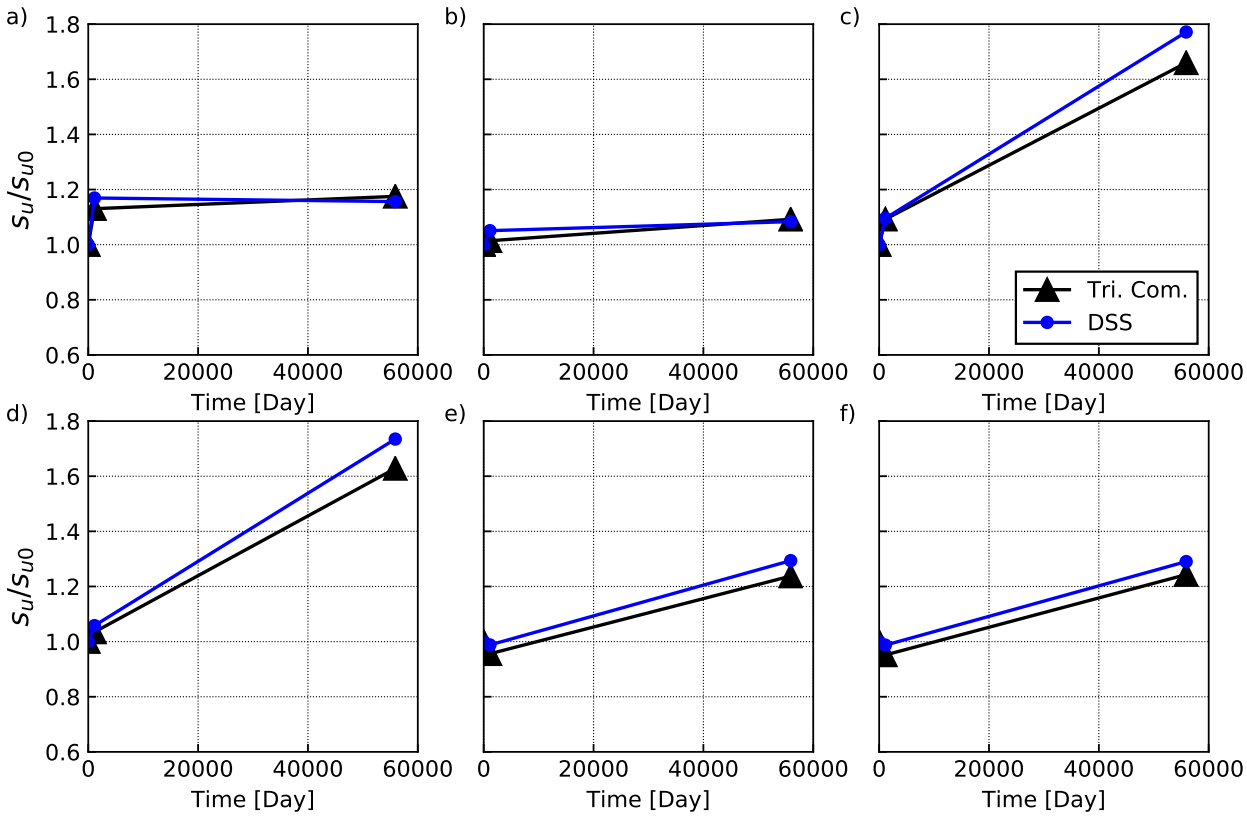

Figure 5.15: *Normalised s_u when μ_i of each soft clay layers have been multiplied by 2, for the depths: 2.5m (a), 3.5m (b), 4.5m (c), 5.5m (d), 7.5m (e) and 9.5m (f).*

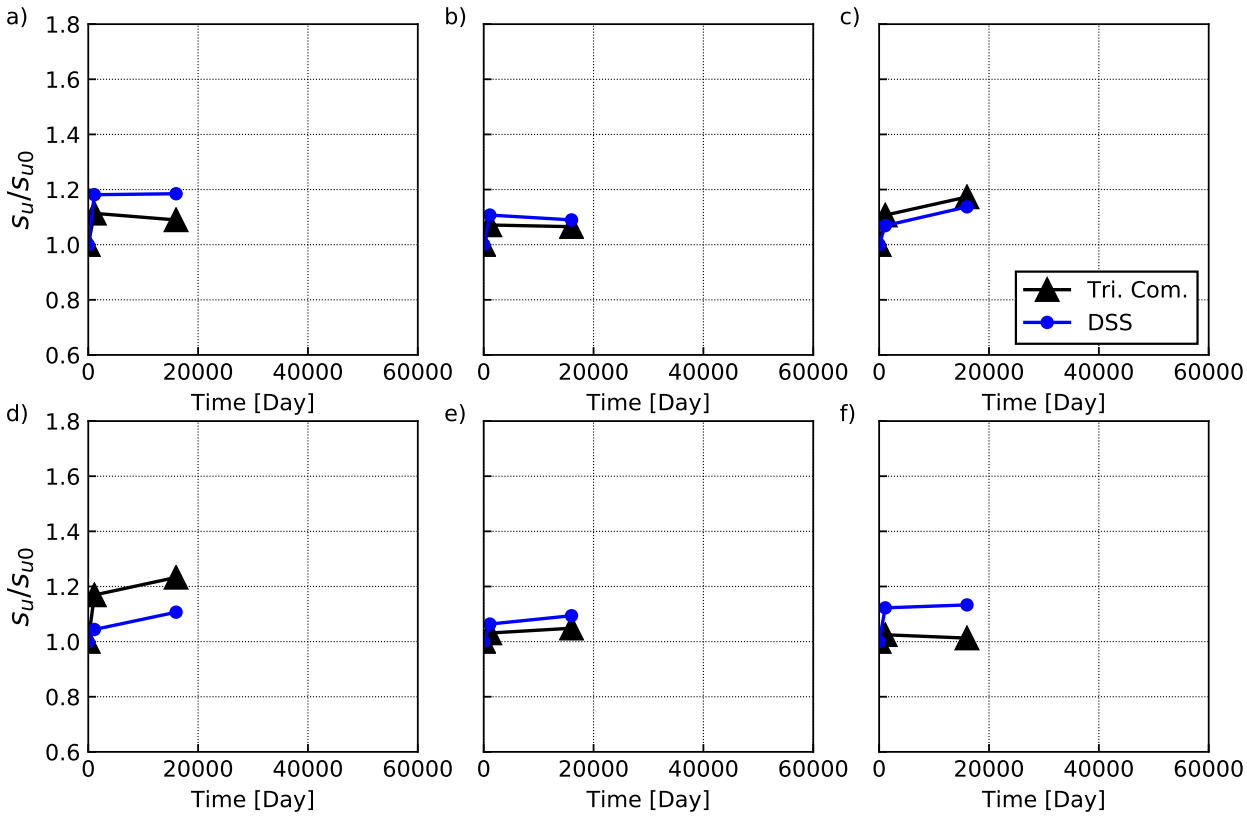

Figure 5.16: *Normalised S_u when μ_i of each soft clay layers have been divided by 2, for the depths: 2.5 m (a), 3.5 m (b), 4.5 m (c), 5.5 m (d), 7.5 m (e) and 9.5 m (f).*

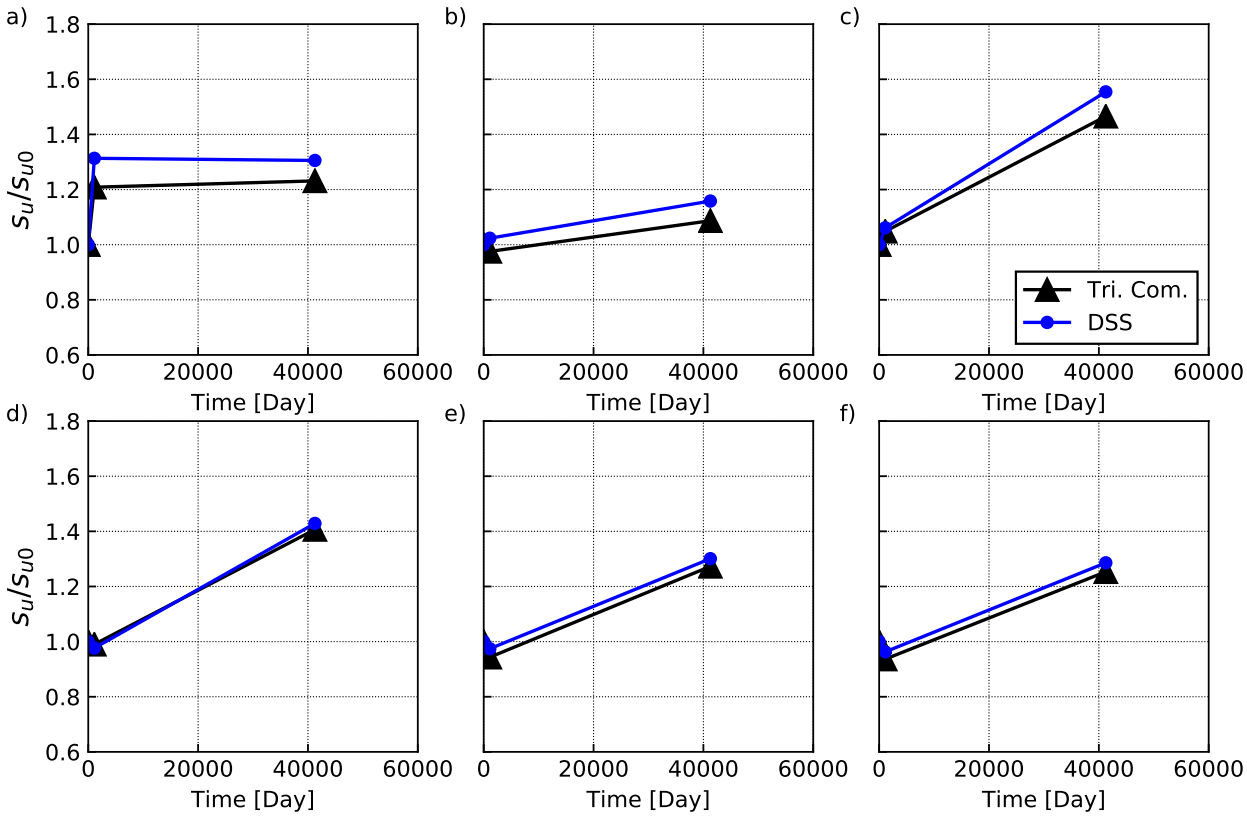

Figure 5.17: *Normalised S_u when pre overburden pressure been decreased by 20 kPa, for the depths: 2.5 m (a), 3.5 m (b), 4.5 m (c), 5.5 m (d), 7.5 m (e) and 9.5 m (f).*

6 Discussion and Conclusions

Haarajoki test embankment was built to study the progress of deformations as a function of time, as well as to study the evolution of the undrained shear strength. For the latter, it has proven to be not the best case study.

In the report, the embankment was modelled with the rate-dependent anisotropic model for sensitive clays, Creep-SCLAY1S. The model was able to capture the initial undrained shear strength profile reasonably well. Overall, the predicted increase in s_u was relatively small for the Haarajoki clay deposit, which is in line with the measurements. The predicted increase was largest in the second clay layer, and the deeper parts of the deposit (8 meters and deeper) were basically unaffected.

The reasons for this can be easily understood. The top part of the deposit is significantly overconsolidated. Additionally, the stiff dry crust may be very effective in redistributing the embankment load. Furthermore, given the high groundwater table, as the embankment settles, it will be subject to the buoyancy effects, and thus the load is reducing. In the lower parts of the deposit, the load increment from the embankment loading is spread sufficiently to not exceed the apparent preconsolidation pressure σ'_c.

The predicted results correspond with the field measurements of the undrained shear strength in Vepsäläinen et al. (2002), which also only showed either no or small increase in the undrained shear strength. According to Vepsäläinen et al. (2002), it was mainly in the top part that there were any measurable changes in soil properties, and even those changes were within the measurement accuracy. Haarajoki is a relatively young embankment (about 23 years), so longer a time frame might be needed to see a bigger increase in s_u.

The case of Haarajoki demonstrates the need for very careful pre-studies before a test embankment is built. One of the problems in Haarajoki is that there are many clay layers with varying stiffness properties. The results demonstrate that large settlements do not necessarily imply that there will be a significant increase in the mobilised undrained shear strength, in particular when the clay is sensitive. Furthermore, based on the simulations in this report, the expected increase in the mobilised undrained shear strength is very sensitive to the apparent preconsolidation pressure as well as the properties controlling the creep rate. Thus, carefully performed incremental loading oedometer tests are required to reliably quantify the creep parameters, as well as the rate-dependent apparent preconsolidation pressure. It is simply not possible to do credible predictions on the time-dependent evolution of the undrained shear strength based on data from CRS tests alone.

The analyses done in the project for the evolution of the undrained shear strength are related to soil elements under the centre line of the embankment. This is a major limitation, as most of the failure mechanism takes place in the areas with significant rotation of principal stresses. Due to the complex stress and fabric rotations, simulations of the mobilised undrained shear strength under the slopes of the embankment would require 3D finite element simulations. As yet, we know far too little on how the rotation of the principal stress axes affects the mobilised undrained strength of natural clays. Exploring that experimentally would require hollow cylinder testing, combined with boundary value interpretation of the test results.

Overall, the appropriate modelling of the system behaviour is important in the analysis of the stability. Furthermore, it can be questioned if stability is the governing design issue for embankments on soft soil. Perhaps in future, we should be more concerned about limiting the (vertical and horizontal) displacements and pore pressures, as those are measurable control

parameters unlike the Factor of Safety. The case of Haarajoki namely demonstrates that an embankment can settle significantly without triggering slope failure. In Eurocode 7, excessive settlements are still considered as failure in ULS, thus an assessment solely based on undrained shear strength, is in fact insufficient.

The only way to ensure that we are able to model the system behaviour as a function of time is to have well-instrumented test embankments in well-characterised sites. A comprehensive instrumentation involves not only surface settlements and pore pressures measurements, but also the vertical settlements as a function of depth. Consolidation of a soft soil deposit is not necessarily uniform. There can be layers in a deposit that compress more than others. For this reason it is necessary to know the vertical strain distributions of the deposit.

From stability point of view, the horizontal movements at several locations, i.e both under the crest and the toe should be measured. Namely, there can be a decrease in the predicted undrained shear strength in the long term, if there are large vertical settlements combined with horizontal movements.

Finally, as a consequence of large vertical settlements, parts of the soil deposit may become submerged (as it settles under the groundwater table), thereby decreasing the effective stress, leading to a lower mobilised undrained shear strength s_u.

References

Amavasai, A., J.-P. Gras, N. Sivasithamparam, M. Karstunen, and J. Dijkstra (2017). Towards consistent numerical analyses of embankments on soft soils. *European Journal of Environmental and Civil Engineering* **8189**, 1–19. ISSN: 19648189. DOI: 10.1080/19648189.2017.1354784. URL: https://doi.org/10.1080/19648189.2017.1354784.

Amavasai, A., N. Sivasithamparam, J. Dijkstra, and M. Karstunen (2018). Consistent Class A & C predictions of the Ballina test embankment. *Computers and Geotechnics* **93**, 75–86. ISSN: 18737633. DOI: 10.1016/j.compgeo.2017.05.025. URL: https://doi.org/10.1016/j.compgeo.2017.05.025.

Berre, T. (2014). Test fill on soft plastic marine clay at Onsøy, Norway. *Canadian Geotechnical Journal* **51**.1, 30–50. DOI: 10.1139/cgj-2012-0479. URL: http://www.nrcresearchpress.com/doi/abs/10.1139/cgj-2012-0479.

– (2018). Test fill brought to failure on soft plastic marine clay at Onsøy, Norway. *Canadian Geotechnical Journal* **55**.4, 563–576. ISSN: 12086010. DOI: 10.1139/cgj-2017-0078.

Bjerrum, L. (1972). "Embankments on soft ground". *Proceedings of the Specialty Conference on Performance of earth and earth-supported structures*, pp. 1–54.

D'Ignazio, M. (2016). "Undrained shear strength of Finnish clays for stability analyses of embankments". PhD thesis. Tampere University of Technology. ISBN: 9789521538049.

Gras, J. P., N. Sivasithamparam, M. Karstunen, and J. Dijkstra (2018). Permissible range of model parameters for natural fine-grained materials. *Acta Geotechnica* **13**.2, 387–398. ISSN: 18611133. DOI: 10.1007/s11440-017-0553-1.

Jaky, J. (1948). "Pressure in silos". *2nd international conference on soil mechanics andfoundation engineering*. Rotterdam.

Karstunen, M., H. Krenn, S.J. Wheeler, M. Koskinen, and R. Zentar (2005). Effect of Anisotropy and Destructuration on the Behaviour of Murro Test Embankment. *International Journal of Geomechanics* **5**.2, 87–97.

Koskinen, M, M Karstunen, and SJ Wheeler (2002). "Modelling destructuration and anisotropy of a natural soft clay". *NUMGE 2002. 5th European Conference Numerical Methods in Geotechnical Engineering*, pp. 11–19.

Koskinen, M and Minna Karstunen (2006). "Numerical modelling of Murro test embankment with S-CLAY1S". *Proc. 6th Eur. Conf. Numer. Methods Geotech. Engng (NUMGE), Graz, Austria*, pp. 455–461.

Ladd, C. C., A. J. Whittle, and D. E. Legaspi (1994). "Stress-Deformation Behavior of an Embankment on Boston Blue Clay". *Vertical and Horizontal Deformations of Foundations and Embankments Volume*. Ed. by A. T. Yeung and G. Y. Felio. Vol. 2, pp. 1730–1759. ISBN: 078440027X.

Larsson, Rolf and Håkan Mattsson (2003). *Settlements and shear strength increase below embankments long term observations and measurement of shear strength increase by seismic cross-hole tomography*. Tech. rep. Swedish Geotechnical Institute.

Lehtonen, V. J., C. L. Meehan, T. Länsivaara, and J. N. Mansikkamäki (2015). Full-scale embankment failure test under simulated train loading. *Géotechnique* **65**.12, 961–974. ISSN: 0016-8505. DOI: 10.1680/geot.14.P.100. URL: http://www.icevirtuallibrary.com/content/article/10.1680/geot.14.P.100.

Leoni, M., M. Karstunen, and P. A. Vermeer (2008). Anisotropic creep model for soft soils. *Geotechnique* **58**.3, 215–226. ISSN: 00168505. DOI: 10.1680/geot.2008.58.3.215.

Lojander, Matti and Pauli Vepsäläinen (2001). *Haarajoen koepenkereen painumalaskentakilpailu: loppuraportti*. Tiehallinto.

Lundström, Karin and Björn Dehlbom (2019). *Egenskapsförändringar med tid under befintliga bankar. Huvudrapport. BIG A2016-10*. Tech. rep. Swedish Geotechnical Institute.

Näätänen, P. V. and M. Lojander (1998). "Finite element calculations on Haarajoki test embankment". *Application of Numerical Methods to Geotechnical Problems*. Ed. by A. Cividini. Udine, pp. 151–160.

Olsson, M. (2010). "Calculating long-term settlement in soft clays". Licentiate Thesis. Chalmers University of Technology, p. 111.

Optum G2 (2020). *Finite element program for geotechnical analysis, Optum Computational Engineering*. URL: http://www.optumce.com.

Rochelle, P. La, B. Trak, F. Tavenas, and M. Roy (1974). Failure of a Test Embankment On a Sensitive Champlain Clay Deposit. *Canadian Geotechnical Journal* **11**.1, 142–164. ISSN: 0008-3674.

Sivasithamparam, N., M. Karstunen, and P. Bonnier (2015). Modelling creep behaviour of anisotropic soft soils. *Computers and Geotechnics* **69**, 46–57. ISSN: 0266-352X. DOI: 10.1016/j.compgeo.2015.04.015. URL: http://dx.doi.org/10.1016/j.compgeo.2015.04.015.

Tavenas, F., P. Jean, P. Leblond, and S. Leroueil (1983). The permeability of natural soft clays. Part II: Permeability characteristics F. *Canadian Geotechnical Journal* **20**.4, 645–660. DOI: 10.1139/t83-072.

Vepsäläinen, Pauli, Matti Lojander, and Mirva Koskinen (2002). *Haarajoen koepenger: maaperän lujittumistutkimus*. Tech. rep. in Finnish.

Wheeler, Simon J., Anu Näätänen, Minna Karstunen, and Matti Lojander (2003). An anisotropic elastoplastic model for soft clays. *Canadian Geotechnical Journal* **40**.2, 403–418. ISSN: 00083674. DOI: 10.1139/t02-119.

Yildiz, A., M. Karstunen, and H. Krenn (2009). Effect of anisotropy and destructuration on behavior of Haarajoki test embankment. *International Journal of Geomechanics* **9**.June, 153–168. DOI: 10.1016/j.buildenv.2006.10.027.

Zwanenburg, C., E. J. Den Haan, G. A. M. Kruse, and A. R. Koelewijn (2012). Failure of a trial embankment on peat in Booneschans, the Netherlands. *Géotechnique* **62**.6, 479–490. DOI: 10.1680/geot.9.P.094. URL: http://www.icevirtuallibrary.com/doi/10.1680/geot.9.P.094.

BIG – Branschsamverkan i grunden
Forskningsprogram för effektiv och säker grundläggning av vägar och järnvägar

BIG

BIG – Branschsamverkan i grunden - är ett forskningsprogram för effektiv och säker grundläggning av transportsystemets infrastruktur. Programmet etablerades under senhösten 2013, och påbörjade sin verksamhet den 1 januari, 2014.

Målsättningen är att sänka kostnader för byggande och underhåll av transportsystemets infrastruktur genom ett långsiktigt och systematiskt utvecklingsarbete inom geoteknikområdet.

I BIG samverkar Trafikverket, Chalmers tekniska högskola, Luleå tekniska universitet, Kungliga tekniska högskolan och Statens geotekniska institut.

Resultat från BIG projekt publiceras i vetenskapliga artiklar och parternas egna rapportserier. Alternativt så publiceras rapporterna i denna gemensamma BIG rapport serie.

Publicerade rapporter

A2014:03	Deformationer i undergrund – Litteratursammanställning och analys
A2014:07	Grundvattensänkning i morän
A2014:13	Höghastighetsspår i Sverige – på bank
A2014:14	On the fundamental relation between soil creep and cyclic pile-soil response
A2016:05	Modelling deformations below high-speed rail
A2017:07	Dynamic response of transition zone on soft clay
A2017:10	Effects of climate change on slopes in sensitive clay
A2017:14	Changes in undrained shear strength as a function of time under embankments